FMRP Interacts with C/D Box snoRNA in the Nucleus and Regulates Ribosomal RNA Methylation

iScience

CellPress

Article

FMRP Interacts with C/D Box snoRNA in the Nucleus and Regulates Ribosomal RNA Methylation

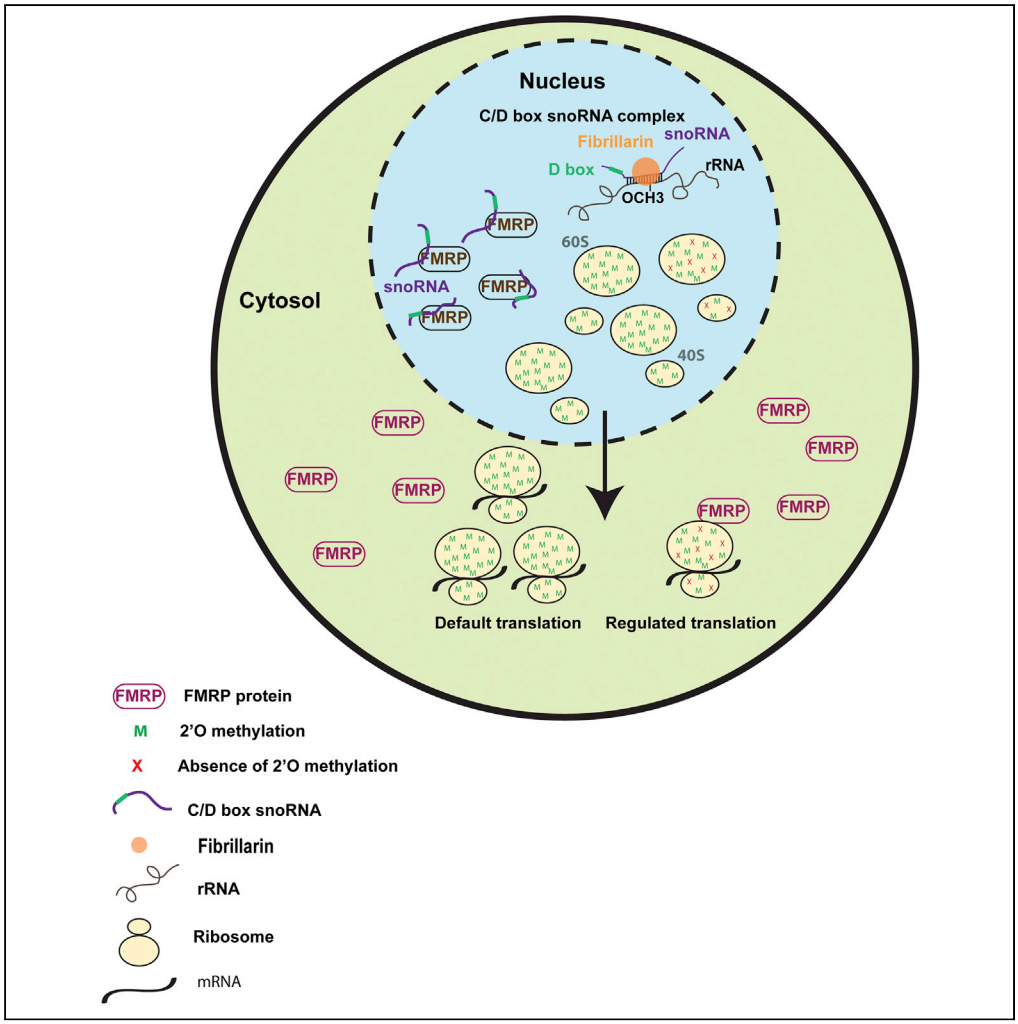

Michelle Ninochka D'Souza, Naveen Kumar Chandappa Gowda, Vishal Tiwari, ..., Akash Gulyani, Dasaradhi Palakodeti, Ravi S. Muddashetty

ravism@instem.res.in

HIGHLIGHTS

FMRP binds to C/D Box snoRNAs in the nucleus

Differential 2'O-methylation on rRNA contributes to ribosome heterogeneity in a cell

2'O-Methylation pattern on ribosomal RNA is altered in the absence of FMRP

FMRP recognizes 2'O-methylation on rRNA, which may determine interaction with ribosomes

D'Souza et al., iScience 9, 399–411
November 30, 2018
https://doi.org/10.1016/j.isci.2018.11.007

iScience

CellPress

Article

FMRP Interacts with C/D Box snoRNA in the Nucleus and Regulates Ribosomal RNA Methylation

Michelle Ninochka D'Souza,[1,4,6] Naveen Kumar Chandappa Gowda,[1,6] Vishal Tiwari,[1,2] Rosana Ottakandathil Babu,[1] Praveen Anand,[1] Sudhriti Ghosh Dastidar,[1,5] Randhir Singh,[1] Bhuvaneish Selvaraja,[3] Rakhi Pal,[1] Arati Ramesh,[2] Sumantra Chattarji,[1,2,3] Siddharthan Chandran,[1,3] Akash Gulyani,[1] Dasaradhi Palakodeti,[1] and Ravi S. Muddashetty[1,7,*]

SUMMARY

FMRP is an RNA-binding protein that is known to localize in the cytoplasm and in the nucleus. Here, we have identified an interaction of FMRP with a specific set of C/D box snoRNAs in the nucleus. C/D box snoRNAs guide 2'O methylations of ribosomal RNA (rRNA) on defined sites, and this modification regulates rRNA folding and assembly of ribosomes. 2'O methylation of rRNA is partial on several sites in human embryonic stem cells, which results in ribosomes with differential methylation patterns. FMRP-snoRNA interaction affects rRNA methylation on several of these sites, and in the absence of FMRP, differential methylation pattern of rRNA is significantly altered. We found that FMRP recognizes ribosomes carrying specific methylation patterns on rRNA and the recognition of methylation pattern by FMRP may potentially determine the translation status of its target mRNAs. Thus, FMRP integrates its function in the nucleus and in the cytoplasm.

INTRODUCTION

Fragile X mental retardation protein (FMRP) is an RNA-binding protein, loss of which leads to fragile X syndrome (Santoro et al., 2012). FMRP is recognized as a translation modulator, and its role in metabotropic glutamate receptor (mGluR) signaling is extensively studied. Dysregulated synaptic translation in the absence of FMRP is thought to be responsible for majority of the phenotypes in fragile X syndrome (Bassell and Warren, 2008; Muddashetty et al., 2007, 2011; Richter et al., 2015). FMRP is also shown to have an important role in neuronal development particularly during neuronal differentiation. The absence of FMRP is reported to affect the maintenance of pluripotency, cell fate choice and rate of progression to the neuronal lineages both in animal and human stem cell models (Li and Zhao, 2014; Luo et al., 2010; Telias et al., 2013). Thus, FMRP-mediated regulation of translation is likely to be more global than confined to the synapse. However, the mechanism of FMRP-mediated translation regulation beyond the synapse is not understood.

FMRP is present in the cytosol as well as in the nucleus and localizes to the distal compartments in neurons. A significant amount of FMRP has been reported to be present in the nuclear and nucleolar compartments in neurons and other cell types (Eberhart et al., 1996; Feng et al., 1997b; Fridell et al., 1996; Kim et al., 2009; Taha et al., 2014). However, the function of FMRP in nucleus still remains unexplained. Since it has both nuclear localization and nuclear export signals, FMRP is proposed to be involved in the shuttling of its target mRNAs between the nucleus and cytosol (Kim et al., 2009). A mutation in the nuclear localization signal was also reported to cause fragile X-like syndrome (Collins et al., 2010). In addition, there is an intriguing possibility that FMRP might interact with a distinct class of RNA in the nuclear/nucleolar compartments and play a crucial role in global translation regulation.

Translational regulation by FMRP has been reported through its direct interaction with the 60S subunit of the ribosome (Chen et al., 2014; Khandjian et al., 1996). A mutation affecting FMRP's interaction with ribosomes leads to a severe form of mental retardation (Feng et al., 1997a; Myrick et al., 2014), whereas its interaction with mRNAs is not affected by this mutation. According to these evidences, we postulate that FMRP has an important function in the nucleus, which could modulate its function in the cytoplasm. Here, we report an interesting interaction of FMRP with a subset of small nucleolar RNAs (snoRNAs) in the nuclear compartment

[1]Institute for Stem Cell Biology and Regenerative Medicine, Bengaluru 560065, India

[2]National Centre for Biological Sciences, Bengaluru, Karnataka 560065, India

[3]Centre for Neuroregeneration, University of Edinburgh, Edinburgh EH16 4SB, UK

[4]The University of Trans-Disciplinary Health Sciences & Technology (TDU), Bengaluru, Karnataka 560064, India

[5]Manipal Academy of Higher Education, Madhav Nagar, Manipal, Karnataka 576104, India

[6]These authors contributed equally

[7]Lead Contact

*Correspondence: ravism@instem.res.in

https://doi.org/10.1016/j.isci.2018.11.007

of human embryonic stem cells (hESCs) and neuronal precursor cells (hNPCs) derived from these hESCs. FMRP's interaction with snoRNAs contributes to differential methylation of rRNA, generating ribosome heterogeneity. The absence of FMRP results in an alteration of this methylation pattern. On the other hand, FMRP also recognizes specific methylation patterns on rRNA and hence marks a subset of ribosomes. Our results identify a nuclear function of FMRP and imply that it can integrate translation regulation between the nucleus and cytoplasm.

RESULTS AND DISCUSSION

FMRP Interacts with a Selected Subset of snoRNAs

To investigate the small RNAs that interact with FMRP during neuronal development, we used human H9 hESCs and H9 neuronal precursor cells (hNPCs) as our model system. H9 hESCs were characterized for pluripotency by immunocytochemistry with the marker OCT4 (Figure 1A), and similarly, hNPCs were characterized for the expression of Nestin (Figure 1B). In H9 hESCs, we show that FMRP interacts with AGO2, a primary component of the miRNA induced silencing complex (miRISC) (Figure 1C) indicating its interaction with microRNA machinery. In our initial observations, other than microRNA, we found another class of RNA (80–100nt) predominantly present in the FMRP immunoprecipitates. To identify this unknown class of small RNAs, we performed an FMRP immunoprecipitation (IP) with H9 hESCs and hNPCs followed by small RNA library preparation from both the microRNA band (30–50 nt) and the higher-molecular-weight band (80–100 nt). An AGO2 IP was used as a positive control to profile the microRNAs (Figure 1D). The libraries were separated on a 6% polyacrylamide gel and showed a prominent band in AGO2 IP at a size of 140 bp representing the population of microRNAs (Figure 1D).

Surprisingly, the prominent band in FMRP IP was identified at a much higher size (around 200 bp) (Figures 1D and S1A). We isolated the bands corresponding to both 140 and 200 bp from the FMRP IP samples and sequenced them separately (Figure 1E). We have included a mouse IgG control in this experiment, and since there was insignificant RNA precipitated with this (Figures 1C and S1B) compared to FMRP IP, it was not further considered for preparation of cDNA library. The band corresponding to 140 bp in FMRP IP majorly contained microRNAs (data not shown) similar to that in the AGO2 IP. Interestingly, the major component of the 200-bp band (corresponding to 80–100 nt RNAs) from the library was C/D box snoRNAs (Figures 1F and 1G). In contrast, AGO2 IP from hESCs and hNPCs showed negligible amount of snoRNA (Figures S1D and S1E) compared with the input (Figure S1C). The library profile of the 200-bp band (corresponding to snoRNA) derived from FMRP IP was similar in both hESCs and hNPCs as depicted by the principal-component analysis plot (Figure 1H). Top snoRNAs associated with FMRP in hESCs are listed in Table S1, and all these snoRNAs are predicted to target and methylate specific sites on 18S or 28S ribosomal RNA.

We validated the interaction of FMRP with snoRNA by performing qPCR for the snoRNAs that were highly enriched in the FMRP IP from H9 hESC lysate (Figure 2A). Our qPCR primers were designed such that an entire snoRNA was amplified from the FMRP IP, suggesting that FMRP interacts with the mature snoRNA (as determined by the sequencing data) rather than the products derived from their further processing (Brameier et al., 2011; Taft et al., 2009). All the selected snoRNA candidates showed a significant enrichment in FMRP IP (pellet/input ratio), compared with the corresponding IgG control (Figure 2A). In contrast, none of the snoRNAs were enriched in the AGO2 pellet (Figure S2B). The small fraction of snoRNA (5%) found in the AGO2 pellet (Figure S1D) could be small RNA derived from further snoRNA processing. The mature full-length snoRNA we tested for were absent in this sample. To confirm that FMRP's interaction with these snoRNAs is specific, we performed IP with an antibody against a different epitope of FMRP (Figure S2A). We further validated FMRP's interaction with target snoRNAs in a different human ESC line (Shef4) (Figure S2C) and in HeLa cells (Figure 2B) as well. Our results indicate that the interaction of FMRP with snoRNAs is a common feature among all the cell types we tested.

FMRP Directly Interacts with C/D Box snoRNA

Our next objective was to test whether FMRP directly interacts with C/D box snoRNAs. To study this, we performed an electrophoretic mobility shift assay with purified full-length human FMRP (Figure S2D). For this we chose SNORD80, one of the top snoRNA candidates which we found to be associated with FMRP in our high-throughput analysis (Tables S1 and S2). SNORD80 was radiolabeled with γ-P-ATP and was incubated with increasing concentrations of FMRP (from 100 nM to 14.6 μM). We observed a shift in

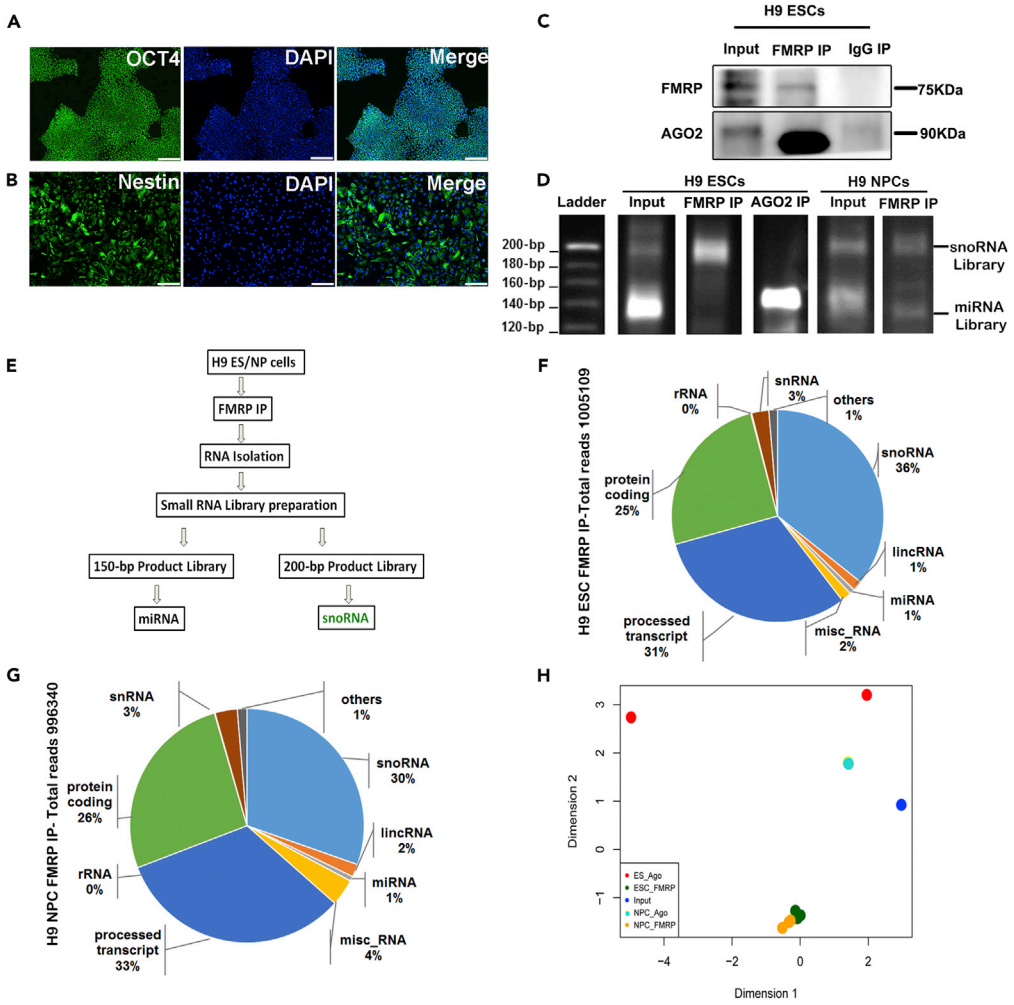

Figure 1. FMRP Interacts with Selected Set of C/D Box snoRNAs in Human ESCs and NPCs

(A) Characterization of H9 hESCs with pluripotency marker OCT4 and nuclear marker DAPI (scale bar, 50 μm).

(B) Characterization of H9 hNPCs with differentiation marker Nestin and nuclear marker DAPI (scale bar, 50 μm).

(C) Immunoblot for FMRP and AGO2 from H9 hESC lysate after FMRP and IgG immunoprecipitation.

(D) Polyacrylamide gels showing mobility of cDNA libraries prepared from RNA extracted after immunoprecipitation with FMRP and AGO2 from H9 hESC and hNPC lysate.

(E) Schematic showing the experimental workflow to identify FMRP-associated small RNAs.

(F) Pie chart showing the distribution of different classes of small RNAs from the sequence obtained from the 200-bp band of the library from H9 hESCs, n = 3.

(G) Pie chart showing the distribution of different classes of small RNAs from the sequence obtained from the 200-bp band of the library from H9 hNPCs, n = 3.

(H) Principal component analysis (PCA) chart indicating clustering of snoRNA libraries in H9 hESCs and H9 hNPCs, hESC FMRP IP n = 3, hNPC FMRP IP n = 3, hESC Input n = 1, and hESC AGO2 IP n = 2.

SNORD80 mobility even with an FMRP concentration of 500 nM (Figure 2C), which was further enhanced in a concentration-dependent manner, indicating a direct interaction of SNORD80 with FMRP. The shift in SNORD80 mobility was completely reversed by incubation with molar excess of unlabeled SNORD80 (Figure 2C-lane 8). This competition was seen only with unlabeled SNORD80 and not with nonspecific bacterial RNA (lane 9 and 10) along with yeast tRNA, which was used in all other lanes thus confirming the specific interaction of SNORD80 with FMRP. Although we demonstrate the direct interaction of FMRP with one of the candidate snoRNAs, we cannot rule out the possibility that FMRP's interaction with C/D box snoRNAs may also be mediated through other snoRNP components or other nuclear FMRP interacting proteins such as NUFIP1 (Bardoni et al., 2003).

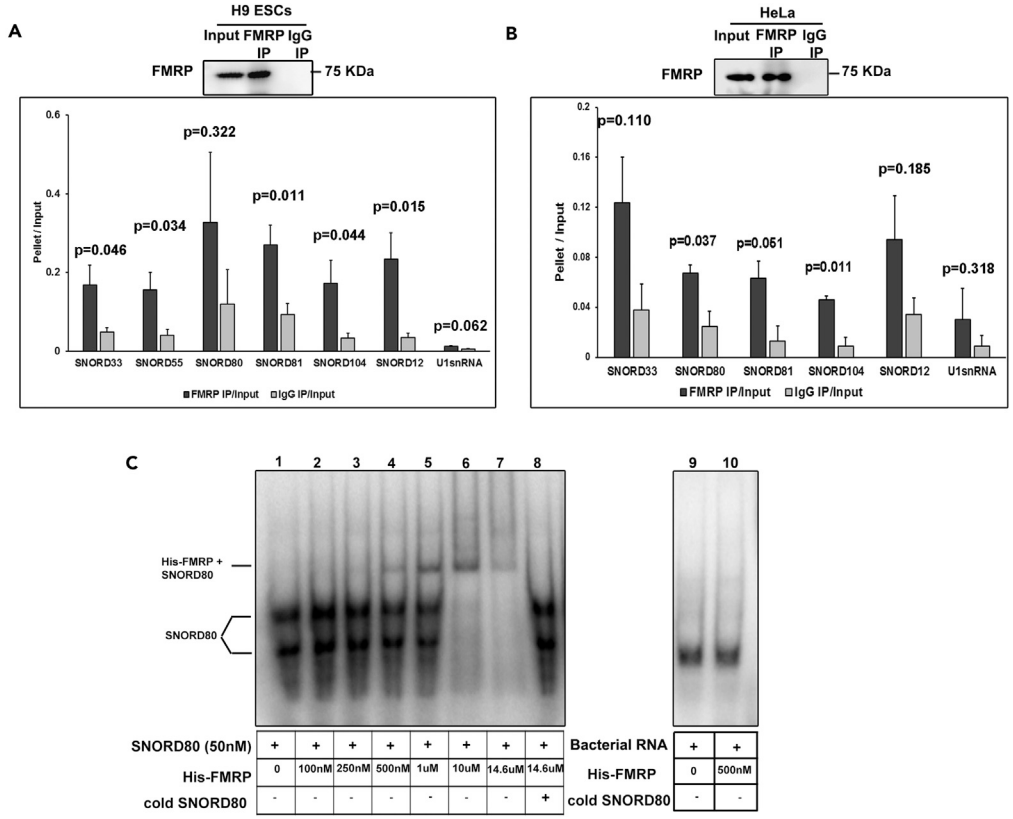

Figure 2. Validation of FMRP Interaction with C/D Box snoRNA

(A) Validation of FMRP-interacting snoRNA in human H9 hESCs by qPCR with representative immunoblot for FMRP IP (n = 6, unpaired Student's t test, mean ± SEM).

(B) Validation of FMRP-interacting snoRNA in HeLa cells by qPCR with representative immunoblot for FMRP IP (n = 4, unpaired Student's t test, mean ± SEM). Also refer Tables S1 and S2.

(C) Electrophoretic mobility shift assay showing shift in mobility of radiolabeled SNORD80 by increasing concentration of His-FMRP. Lane 8 shows a complete abolishment of shift with molar excess of unlabeled (cold) SNORD80 RNA. Lanes 9 and 10 indicated no change in the mobility of His-FMRP with radiolabeled non-specific bacterial RNA. Samples in lanes 9 and 10 were run on a separate gel.

Among the two major classes of snoRNAs involved in rRNA modifications (C/D box snoRNAs that mediate 2-O'methylation and H/ACA box snoRNAs that mediate pseudo-uridylation) (Falaleeva et al., 2017; Henras et al., 2015), we detected only C/D box snoRNAs in the FMRP pellet. We did see a weak higher-molecular-weight band in the cDNA library prepared from the FMRP pellet (Figure S1A); however, we did not find any H/ACA box snoRNA or precursor snoRNA when we sequenced this band (data not shown). Thus, FMRP appears to interact only with C/D box snoRNA, although we cannot completely rule out an interaction with H/ACA box snoRNA in the FMRP pellet. Since H/ACA box snoRNAs possess complex secondary structures, there is a possible bias against them in the cDNA library preparation.

The specific interaction with C/D box snoRNAs indicates that FMRP seems to have an important role in rRNA methylation. These C/D box snoRNAs primarily guide the 2'O methylation on selected ribose sugars on rRNA, which is important for the folding of the rRNA and the assembly of ribosomal proteins (Falaleeva et al., 2017; Sharma and Lafontaine, 2015). Some snoRNAs are also reported to generate smaller RNAs, including microRNAs (Brameier et al., 2011), found in the cytoplasm. Here, we show that FMRP's interaction with snoRNAs is only confined to the nuclear fraction (Figure 3G). Also, it interacts with full-length snoRNAs and not the processed small RNA products of snoRNAs.

A group of snoRNAs without specific targets on rRNA (called orphan snoRNAs) are also known to have a role in mRNA splicing (Kishore and Stamm, 2006). All top snoRNA candidates precipitated with FMRP

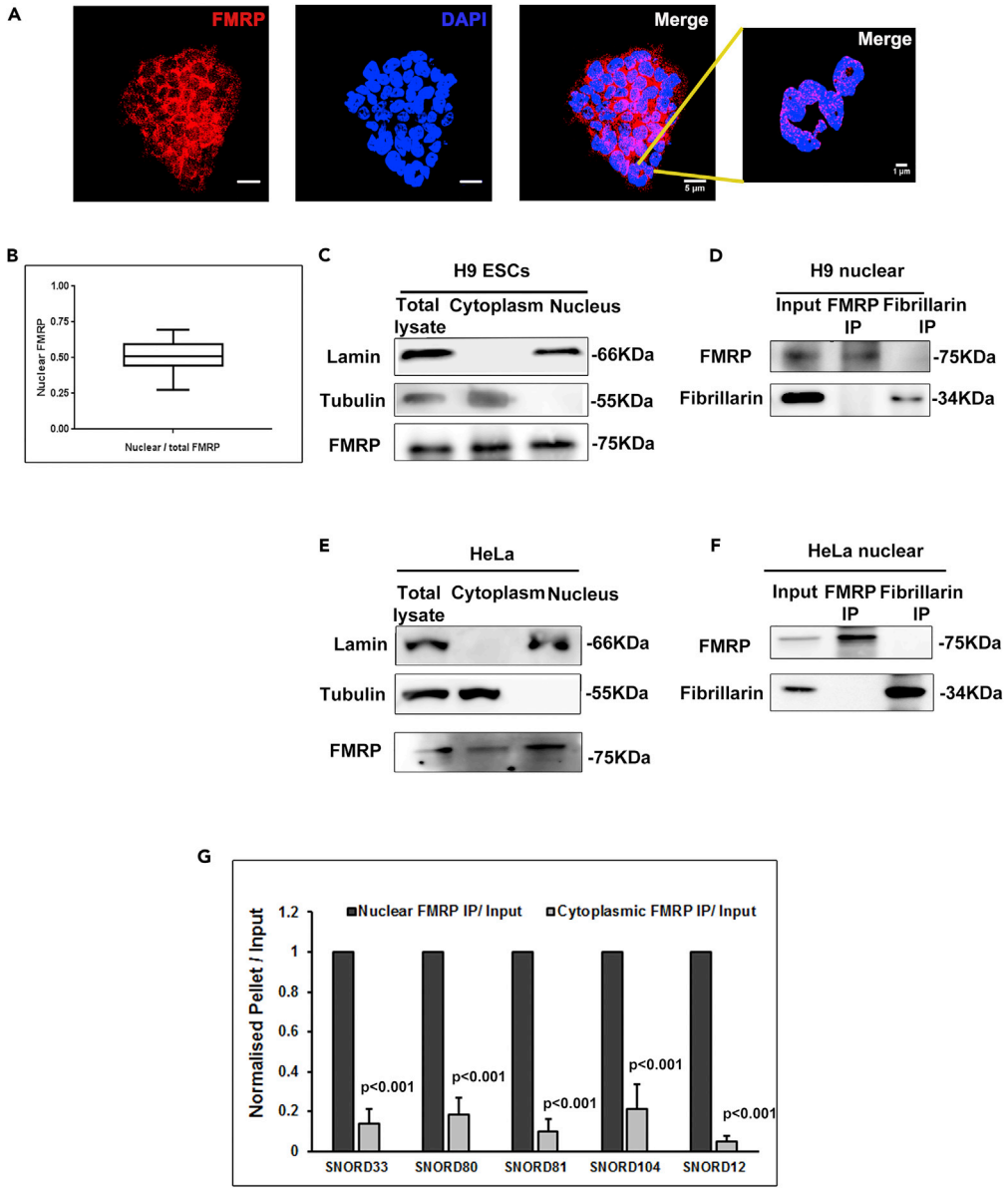

Figure 3. Interaction of Nuclear FMRP with C/D Box snoRNA

(A) Immunostaining of H9 hESCs (blue-DAPI, red-FMRP, and scale bar, 5 μm) followed by segmented images showing nuclear distribution of FMRP (scale bar, 1 μm).

(B) Quantification of nuclear FMRP in H9 hESCs, n = 29 cells.

(C) Immunoblots showing the distribution of FMRP in H9 hESC nuclear and cytoplasmic fractions, Lamin as nuclear marker and Tubulin as cytoplasmic marker.

(D) Immunoblots for FMRP and Fibrillarin followed by FMRP or Fibrillarin immunoprecipitation from nuclear fractions of H9 hESCs.

(E) Immunoblots showing the distribution of FMRP in HeLa nuclear and cytoplasmic fractions with Lamin as nuclear marker and Tubulin as cytoplasmic marker.

(F) Immunoblots for FMRP and Fibrillarin followed by FMRP or Fibrillarin immunoprecipitation from nuclear fractions of HeLa cells.

(G) qPCR for selected snoRNAs after immunoprecipitation with FMRP from nuclear and cytoplasmic lysates of H9 hESCs. Values are the ratio of pellet/input of the cytoplasmic fraction normalized to the pellet/input ratio of the nuclear fraction (n = 3, unpaired Student's t test, mean ± SEM).

have predicted target sites on rRNA, and we did not find any orphan snoRNA enriched in the pellet (Table S1). These results clearly suggest that the interaction of FMRP with snoRNA is likely to have a role in rRNA methylation.

Interaction with snoRNA Is a Function of Nuclear FMRP

Although FMRP is often studied as a cytoplasmic protein, it has a nuclear localization signal, and its localization to the nucleus is reported by several studies (Kim et al., 2009; Taha et al., 2014). Here we show a localization of FMRP in the nucleus of H9 hESCs (Figure 3A) by FMRP immunostaining overlaid with DAPI, a nuclear marker. Similarly, we observed FMRP's localization in the nucleus of Neuro2A (Figure S3A), HeLa (Figure S3B), rat cortical neurons (Figure S3C), and rat astrocytes (Figure S3D) confirming that FMRP is present both in the nucleus and cytoplasm of the all the cell types that we studied. We quantified the percentage of FMRP in the nucleus based on DAPI staining (Figure 3B) and found that nearly 50% of FMRP localized in the nucleus of hESCs. Since the nucleus of ESCs is relatively large, we expect the ratio of nuclear to cytoplasmic FMRP to be lower in other cell types (Figures S3A–S3D). We also confirmed that FMRP's localization in the nucleus is specific through immunostaining with an antibody raised against a different epitope of FMRP (Figure S3E). To establish the compartment-specific localization of FMRP, we used nuclear and cytoplasmic fractions from H9 hESCs (Bensaddek et al., 2016) and probed for the presence of FMRP. The purity of the fractionation was validated by LaminB1 and α-Tubulin as nuclear and cytoplasmic markers respectively (Figure 3C). FMRP was found to be present in both nuclear and cytoplasmic fractions (Figure 3C).

The sequence between the C and D′ box (or C′ and D) is complementary to a specific region on rRNA, and this complementarity determines the site to be methylated (Cavaille et al., 1996). RNA-binding proteins forming the snoRNP complex are recruited to these sites by C/D box snoRNAs, and 2′O-methylation is carried out by a nucleolar-specific methyltransferase, Fibrillarin (Shubina et al., 2016). Since FMRP has a putative nucleolar localization signal and has been shown to localize to the nucleolus (Taha et al., 2014), we tested whether it interacts with Fibrillarin. For this, we probed for the presence of Fibrillarin in FMRP immunoprecipitates from the nuclear fraction of H9 hESCs. We did not see a co-precipitation of Fibrillarin with FMRP (Figure 3D). Similarly, we did not see FMRP in the Fibrillarin immunoprecipitate (Figure 3D). We tested for this interaction in nuclear extracts of HeLa (Figures 3E and 3F) and Neuro2A (Figure S3F) and did not find FMRP co-precipitating with Fibrillarin in any of these experiments. These results strongly suggest that FMRP and Fibrillarin are likely to be present in separate RNPs, although both interact with snoRNA. Finally, to confirm that the interaction of FMRP with snoRNA is in the nucleus, we performed an FMRP IP from H9 hESC nuclear and cytoplasmic fractions followed by qPCR for selected target snoRNAs. We found that these snoRNAs are significantly enriched in immunoprecipitates from nuclear fractions compared with cytoplasmic fractions (Figures 3G and S3G). Thus, FMRP-snoRNA interaction is primarily in the nuclear compartment and seems to be distinct from Fibrillarin-containing snoRNPs. FMRP may sequester specific snoRNAs and control their availability to rRNA methylation machinery and regulate the extent of methylation. Similarly, other RNA-binding proteins might be involved in regulating rRNA methylation through their interaction with snoRNAs cumulatively leading to the differential rRNA methylation.

Differential 2′O-Methylation of rRNA in Human ESCs

So far 106 methylation sites have been identified on human rRNA (Falaleeva et al., 2017; Incarnato et al., 2017; Machnicka et al., 2013). Recently it was reported that the differential methylation of selected sites on rRNA can give rise to ribosome heterogeneity as demonstrated in HeLa cells (Krogh et al., 2016). To establish the differential rRNA methylation in human ESCs, we estimated the extent of rRNA methylation of known sites in Shef4 hESCs using the recently developed high-throughput RiboMeth sequencing method (Marchand et al., 2017). In this method, ribosomal RNA extracted from hESCs was subjected to partial alkaline hydrolysis, followed by library preparation and sequencing (See Transparent Methods section). The sequenced data were analyzed to estimate the extent of methylation using a previously described (Krogh et al., 2016) bioinformatics pipeline (Figure S4A). In our assay we detected 97 sites in Shef4 hESC rRNA. A majority of the sites are completely methylated (methylation index close to 1); however, 9 sites on 18S rRNA (Figure 4A) and 15 sites on 28S rRNA were only partially methylated (methylation index significantly lower than 1) (Figure 4B) as reflected in Table S3. The extent of methylation on these sites varied from a methylation index of 0.6 to 0.9 (Figures 4A and 4B), which denotes that these sites are methylated in 60%–90% of the ribosomes, whereas they are unmethylated in the remaining 10%–40% of the ribosomes. The heterogeneity of rRNA methylation we observed in hESCs is distinct from that of HeLa cells as reported previously (Krogh et al., 2016).

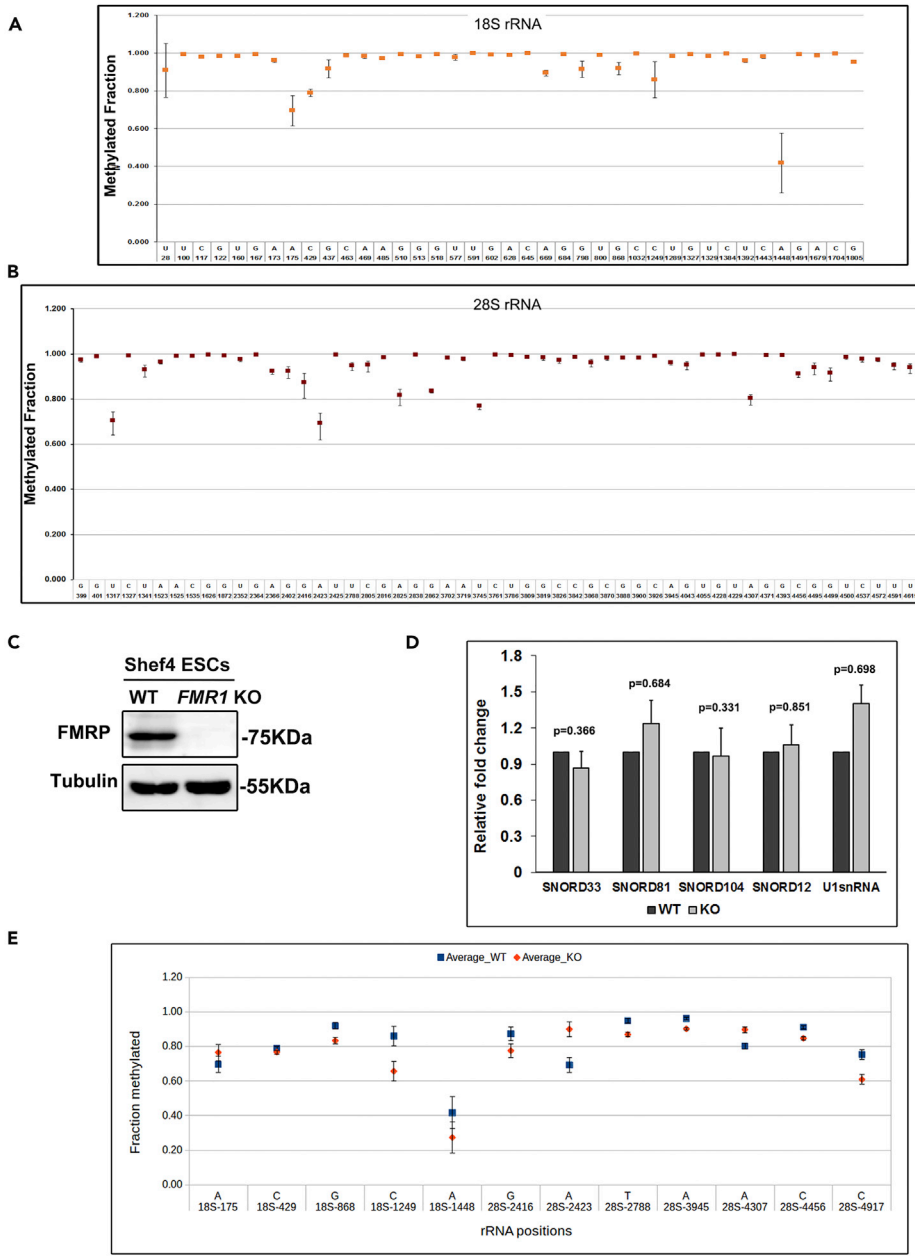

Figure 4. Ribosomal RNA 2′O-Methylation Pattern in Shef4 and Shef4 *FMR1* KO hESCs

(A) Methylation index of the sites on 18S rRNA in Shef4 hESCs. The x axis represents the respective methylation position on 18S rRNA, and y axis represents the fraction methylated, n = 3.

(B) Methylation index of the sites on 28S rRNA in Shef4 hESCs. The x axis represents the respective methylation position on 28S rRNA, and y axis represents the fraction methylated, n = 3.

(C) Immunoblots showing absence of FMRP in Shef4 *FMR1* KO hESCs with Tubulin as the control.

(D) Change in levels of top snoRNA candidates in Shef4 WT and Shef4 *FMR1* KO hESCs by qPCR (n = 5, unpaired Student's t test, mean ± SEM).

(E) Sites in 18S and 28S rRNA that show 5% or more difference in the methylation index between Shef4 hESCs and Shef4 *FMR1* KO hESCs (n = 3, mean ± SEM).

Absence of FMRP Alters the rRNA 2′O-Methylation Pattern in Human ESCs

We observe that FMRP interacts with a specific subset of C/D box snoRNAs (Table S1), and we wanted to test if the absence of FMRP will have any effect on the level of its target snoRNAs at steady state. For this we

generated Shef4 *FMR1* knockout (KO) hESCs using the CRISPR-Cas9 system (Figures 4C and S4B–S4E) and performed a qPCR for these candidate snoRNAs. Surprisingly, at steady state, we did not see any significant change in the level of FMRP target snoRNAs in *FMR1* KO cells (Figure 4D). Since most of the snoRNAs we found associated with FMRP were C/D box snoRNA, we studied the impact of this interaction (FMRP-snoRNA) by looking at 2′O methylation in Shef4 wild-type (WT) and Shef4 *FMR1* KO hESCs (Figures 4E, S4F, and S4G). We performed a high-throughput RiboMethSeq from WT and *FMR1* KO hESCs as described previously. On comparing the methylation profile between WT and KO cells, we found that the sites that were fully methylated in WT (methylation index 1) were unaffected in the absence of FMRP (Figures S4F and S4G). Interestingly, many sites in 18S and 28S rRNA that were partially methylated in WT hESCs were significantly altered in the absence of FMRP (Figure 4E and Table S3).

We independently validated the change in methylation of rRNA in the absence of FMRP for selected sites (Figure 5A) by a qPCR-based method called RTL-P (Dong et al., 2012) (Figure S5A). RTL-P has been previously used to identify the differential methylation of rRNA (Dong et al., 2012), and we have further tested the validity of this assay (Figures S5A–S5G). This method involves the amplification of PCR products under high and low dNTP concentrations for each primer set. There are two forward primers, one positioned upstream (P1) and other downstream (P2) of the methylation site. Amplification was done using a reverse primer (P3) downstream of the methylation site (Figure S5A). For RTL-P we have considered the smaller PCR product (from P2 and P3) as our control in both high and low dNTP conditions (since it is unaffected by methylation). Then we have quantified the larger PCR product (from P1 and P3) at similar conditions and normalized it to its respective smaller PCR product (Figures S5B and S5C). Example of RTL-P analysis for a given site has been provided in Transparent Methods. We have validated two selected sites 401 (complete methylation) and 4917 (partial methylation) through RTL-P. The PCR products were run on a gel, and the bands corresponding to the upstream product (*) were selectively cut out and cloned into a bacterial vector (Figures S5B and S5C) for Sanger sequencing (Figures S5F and S5G). Furthermore, we validated site 4917 in WT and in *FMR1* knockdown HeLa cells. We observe that the intensity of the amplicon generated for the knockdown samples under low dNTPs is lesser compared to that of the WT (Figures S5D and S5E). Here, we clearly show that under low and high dNTP conditions, we observe the PCR reaction stopping downstream and upstream of the methylation site as expected (Figures S5F and S5G).

We chose sites for RTL-P validation based on our high-throughput sequencing as well as sites that were targeted by our top snoRNA candidates. Our RTL-P results were similar to that of the RiboMethSeq. Sites 429, 2416 and 4917 are significantly hypo-methylated in *FMR1* KO compared to WT. Site 4307 was significantly hyper-methylated in *FMR1* KO, whereas the methylation on site 401 was unaltered (Figure 5A). Apart from these, we also show that site 3680 (targeted by FMRP associated SNORD88A) is significantly hyper-methylated in the *FMR1* KO, although there was no difference in RiboMethSeq (Figure 5A). These results confirm that absence of FMRP has a significant impact on the methylation status of specific rRNA sites.

Heterogeneity among ribosomes is an emerging concept and provides a new dimension for translation regulation (Lafontaine, 2015; Shi et al., 2017). Modifications on rRNA, including snoRNA-guided methylation, are proposed to play an important role in contributing to heterogeneity (Falaleeva et al., 2017). However, the mechanism by which differential modification of rRNA occurs is not explored. Our work for the first time defines an interaction of an RNA-binding protein, FMRP, with a specific subset of C/D box snoRNAs. This interaction may have an influence in regulating rRNA methylation in humans. In the absence of FMRP, methylation was altered for 12 (5 on 18S rRNA and 7 on 28S rRNA) of 28 differentially methylated sites as identified by RiboMethSeq. Interestingly, sites that show an altered methylation in the absence of FMRP are the ones that also show partial methylation in the control (WT) hESCs (methylation index less than 1). This implies that FMRP has an important role in differential methylation of rRNA and has a significant contribution in generating ribosome heterogeneity.

Acute Knockdown or Overexpression of FMRP Alters rRNA 2′O-Methylation Pattern

To verify that the change in 2′O-methylation observed is FMRP specific, we acutely knocked down FMRP (48 hr with siRNA, Figures 5B, 5C, and S5H) and overexpressed FLAG-FMRP (24 hr Figures 5H and S5I) in HeLa cells. Following FMRP knockdown or overexpression, we estimated the methylation of rRNA on selected sites through RTL-P (Figures 5D–5F and 5H–5J). On acute knockdown of FMRP, we observed hypo-methylation on the sites 2416, 4456, and 4917 (Figure 5E). The hypo-methylation of these sites on

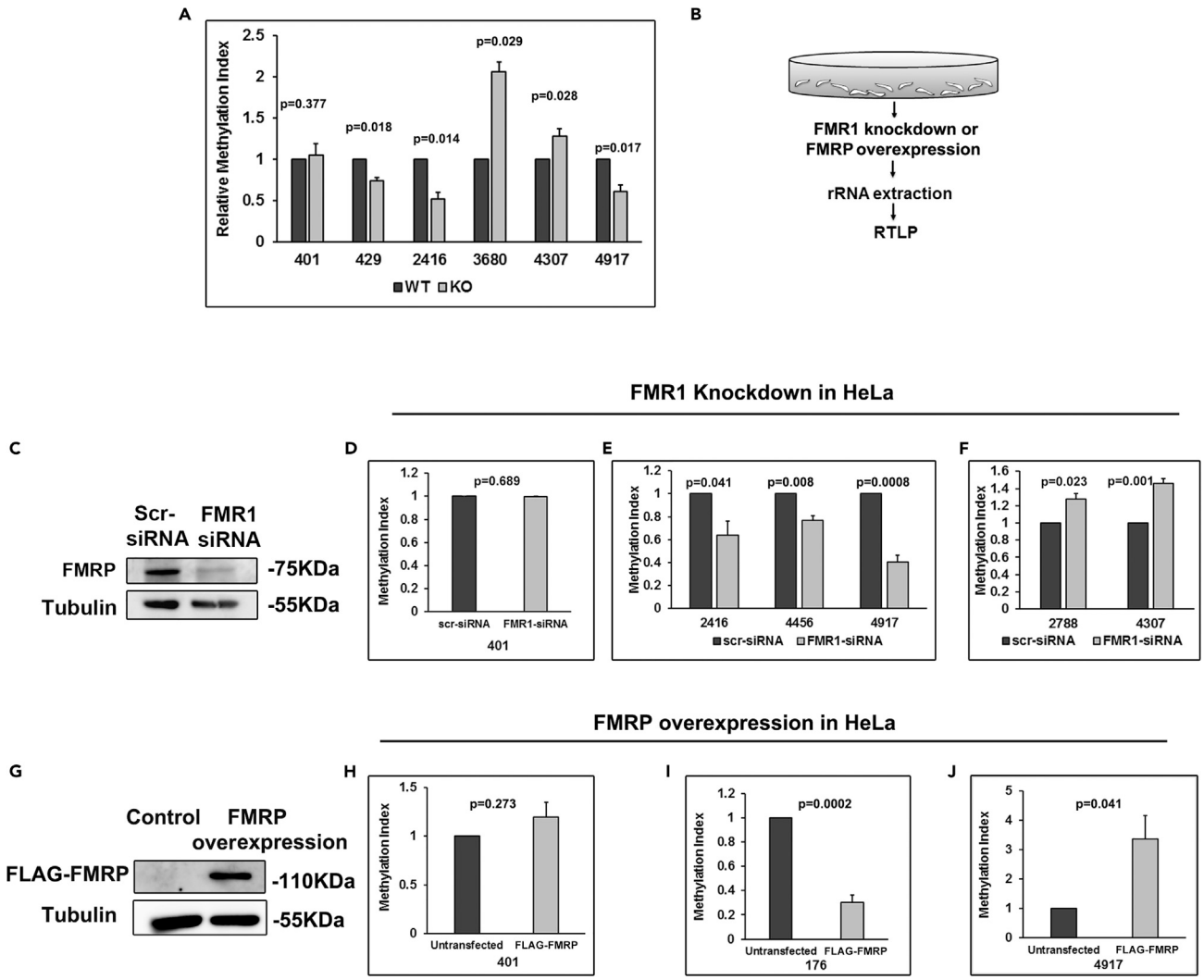

Figure 5. Validation of Change in rRNA 2′O-Methylation Pattern by FMRP

(A) RTL-P for selected sites on 18S and 28S rRNA to show differences in methylation in Shef4 WT and Shef4 *FMR1* KO hESC lysate (n = 3, unpaired Student's t test, mean ± SEM).

(B) Schematic for reverse transcription followed by PCR (RTL-P) on *FMR1* knockdown or FMRP overexpression in HeLa cells.

(C) Representative immunoblots for FMRP showing its knockdown in HeLa cells with Tubulin as a control.

(D–F) RTL-P for selected sites showing the change in 2′O-methylation on *FMR1* knockdown in HeLa cells (n = 3, unpaired Student's t test, mean ± SEM).

(G) Representative immunoblots for FMRP showing overexpression of FLAG-FMRP in HeLa cells with Tubulin as a control.

(H–J) RTL-P for selected sites showing the change in 2′O-methylation on overexpression of FLAG-FMRP in HeLa cells (n = 3, unpaired Student's t test, mean ± SEM).

FMRP knockdown is the same as we have identified in *FMR1* KO hESCs both by high-throughput RiboMethSeq (Figure 4E) and RTL-P-based analysis from the same cells (Figure 5A). Sites 2788 and 4307, which showed hyper-methylation in *FMR1* KO hESCs, also showed hyper-methylation on acute knockdown of FMRP in HeLa cells (Figure 5F). These results confirm that the change in methylation in *FMR1* KO hESCs could be reproduced by acute knockdown of FMRP. In contrast, the effect of acute overexpression of FMRP was more complex. One of the sites (176), which showed hyper-methylation in *FMR1* KO hESCs (Figure 4E), showed a hypo-methylation on FMRP overexpression (Figure 5I) in HeLa cells. Similarly, a site (4917) that showed hypo-methylation in *FMR1* KO hESCs showed hyper-methylation on FMRP overexpression (Figure 5J), clearly indicating that the presence or absence of FMRP is the direct cause of change in methylation. Site 401, which was unaffected in *FMR1* KO hESCs, remained unchanged (with respect to its methylation) on FMRP knockdown or overexpression in HeLa cells (Figures 5D and 5H). Although acute

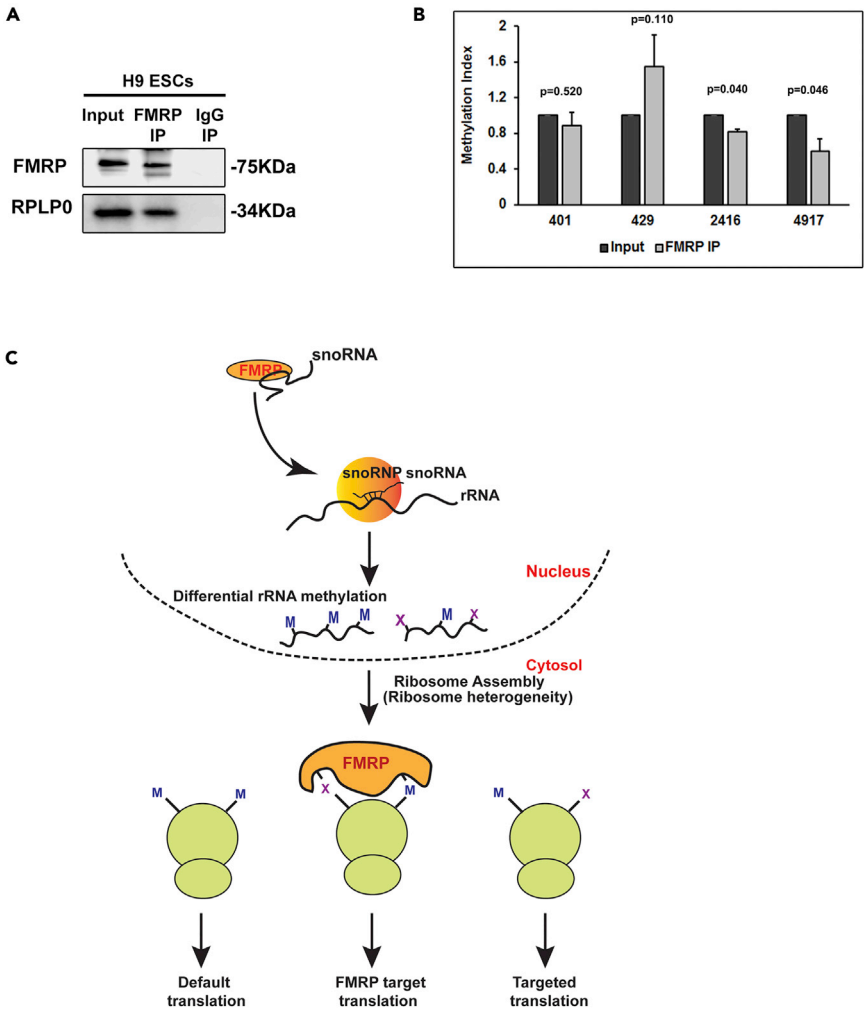

Figure 6. Recognition of rRNA 2′O-Methylation by FMRP

(A) Immunoblots showing the presence of ribosomal protein RPLP0 in FMRP immunoprecipitate from H9 hESC nuclear fractions.

(B) Relative methylation index of H9 hESC rRNA from FMRP IP normalized to input by RTL-P (n = 3–4, unpaired Student's t test, mean ± SEM).

(C) Model illustrating the role of FMRP in regulating translation through differential rRNA methylation.

knockdown of FMRP reproduces the results of *FMR1* KO, overexpression of FMRP has inconsistent effects. Overexpression may have limited effects owing to saturating concentration of endogenous FMRP.

Overall, our results indicate that absence of FMRP can lead to either hypo- or hyper-methylation on distinct sites. FMRP may sequester specific snoRNAs and control their availability to rRNA methylation machinery and regulate the extent of 2′O-methylation. However, the role of FMRP in controlling status of methylation is unclear; identifying the other components (both protein and RNA) involved is needed to address this issue.

FMRP Recognizes Differential 2′O-Methylation Pattern

We have demonstrated that FMRP interacts with a subset of snoRNAs in the nuclear compartment. In the absence of FMRP, rRNA 2′O-methylation is significantly altered and this affects ribosome heterogeneity. We also show that FMRP interacts with ribosomal proteins (Figure 6A) as also previously reported (Chen et al., 2014) (Simsek et al., 2017). Based on these results we wanted to investigate if FMRP can recognize the 2′O-methylation pattern on ribosomes. For this we performed FMRP immunoprecipitation and

isolated rRNA, which was pulled down with FMRP. We quantified the extent of 2′O-methylation of selected sites on rRNA by RTL-P and compared it with the extent of methylation to ribosomes in the input (Figure 6B). We chose the sites whose methylation is altered in the absence of FMRP. Among them, three sites showed a significant difference in the FMRP pellet compared to the input. Site 429 (18S rRNA) showed a trend of hyper-methylation in the FMRP pellet, whereas sites 2416 and 4917 (28S rRNA) were hypo-methylated compared to the input. Site 401 remained unchanged (Figure 6B). There was no difference in the methylation pattern for these sites in the control IP with IgG (Figure S6B). These results indicate that FMRP binds to the ribosome preferentially when site 429 is methylated in 18S rRNA and 2416 and 4917 are unmethylated in 28S rRNA. Although we show that FMRP interacts with ribosomal proteins in the nuclear fraction (Figure 6A), currently we do not know whether this recognition of rRNA methylation pattern by FMRP happens during the assembly of ribosomes or later. Our initial experiments indicate that FMRP shows a better interaction with rRNA when it is from cell lysate rather than with purified rRNA (Figure S6A).

An interesting possibility is that the heterogeneity influenced by FMRP (in the form of differential rRNA methylation) is recognized by FMRP itself and thus recruits a subset of ribosomes for the translation of its own target mRNAs (Figure 6C-model). Our results indicate that FMRP recognizes differential 2′O-methylation pattern on selected sites of rRNA. Interestingly, there are many G-quartet structures (an RNA motif recognized by FMRP) that lie in close proximity to these rRNA methylation sites, which might be regulated by FMRP (Figure S6C). An altered methylation on these sites could influence the G-quartet structures, which interact with FMRP. We propose this to be the mechanism by which FMRP recognizes ribosomes based on differential rRNA methylation on specific sites (Figure 6C-model).

Limitations of the Study

This study focused on the interaction of FMRP with C/D box snoRNA in the nucleus. Our data suggests that the interaction of FMRP with specific C/D Box snoRNA might affect 2′O-methylation on rRNA. At the mechanistic level, our data can correlate only the levels of FMRP and the consequent change in methylation of specific sites. We show that FMRP and Fibrillarin (rRNA-specific methyltransferase) are in separate complexes, and we do not know the exact molecular mechanism involving the FMRP-snoRNA complex and how it regulates changes in rRNA post-transcriptional modifications in a cell.

We know from our data that FMRP can bind to the ribosome, especially through the RNA component. We propose a putative model describing how the rRNA methylation pattern can be recognized by FMRP based on a bio-informatics prediction, but we currently do not have any experimental evidence to prove that. Our data demonstrates the link between FMRP's interaction with a subset of C/D box snoRNAs and rRNA methylation. Although we have evidence regarding the recognition of specific 2′O-methylation patterns by RNA binding proteins (RBPs) like FMRP, we are yet to understand the correlation between the role of FMRP in rRNA methylation, FMRP's recognition of specific methylation patterns, and translation regulation of specific subset of mRNAs, which is beyond the scope of our manuscript.

METHODS

All methods can be found in the accompanying Transparent Methods supplemental file.

SUPPLEMENTAL INFORMATION

Supplemental Information includes Transparent Methods, six figures, and three tables and can be found with this article online at https://doi.org/10.1016/j.isci.2018.11.007.

ACKNOWLEDGMENTS

The work has been funded by the NeuroStem grant (BT/IN/Denmark/07/RSM/2015-2016), RNAi grant from the Department of Biotechnology (BT/PR8723/AGR/36/776/2013), Centre for Brain Development and Repair (CBDR) grant (BT/PR11434/MED/30/1389/2014), India. R.S. acknowledges his DBT-RA fellowship for the same. We would like to thank the Stem Cell Facility and Central Imaging & Flow Cytometry Facility, InStem. We would like to thank all Muddashetty laboratory members for their suggestions and advice during the course of this work.

AUTHOR CONTRIBUTIONS

Conceptualization - M.N.D., N.K.C.G., V.T., and R.S.M.; Validation - M.N.D., N.K.C.G., V.T., and A.R.; Formal Analysis - R.O.B., P.A., M.N.D., N.K.C.G., V.T., D.P., and R.S.M.; Resources - B.S., R.S., R. P., A.G., S. Chandran, S. Chattarji, and R.S.M; Writing, Review & Editing, M.N.D., N.K.C.G., V.T., and R.S.M.; Funding, R.S.M.; Supervision, R.S.M.

DECLARATION OF INTERESTS

The authors declare no competing interests.

Received: May 9, 2018
Revised: September 28, 2018
Accepted: November 1, 2018
Published: November 30, 2018

REFERENCES

Bardoni, B., Willemsen, R., Weiler, I.J., Schenck, A., Severijnen, L.A., Hindelang, C., Lalli, E., and Mandel, J.L. (2003). NUFIP1 (nuclear FMRP interacting protein 1) is a nucleocytoplasmic shuttling protein associated with active synaptoneurosomes. Exp. Cell Res. *289*, 95–107.

Bassell, G.J., and Warren, S.T. (2008). Fragile X syndrome: loss of local mRNA regulation alters synaptic development and function. Neuron *60*, 201–214.

Bensaddek, D., Nicolas, A., and Lamond, A.I. (2016). Quantitative proteomic analysis of the human nucleolus. Methods Mol. Biol. *1455*, 249–262.

Brameier, M., Herwig, A., Reinhardt, R., Walter, L., and Gruber, J. (2011). Human box C/D snoRNAs with miRNA like functions: expanding the range of regulatory RNAs. Nucleic Acids Res. *39*, 675–686.

Cavaille, J., Nicoloso, M., and Bachellerie, J.P. (1996). Targeted ribose methylation of RNA in vivo directed by tailored antisense RNA guides. Nature *383*, 732–735.

Chen, E., Sharma, M.R., Shi, X., Agrawal, R.K., and Joseph, S. (2014). Fragile X mental retardation protein regulates translation by binding directly to the ribosome. Mol. Cell *54*, 407–417.

Collins, S.C., Bray, S.M., Suhl, J.A., Cutler, D.J., Coffee, B., Zwick, M.E., and Warren, S.T. (2010). Identification of novel FMR1 variants by massively parallel sequencing in developmentally delayed males. Am. J. Med. Genet. A *152A*, 2512–2520.

Dong, Z.W., Shao, P., Diao, L.T., Zhou, H., Yu, C.H., and Qu, L.H. (2012). RTL-P: a sensitive approach for detecting sites of 2′-O-methylation in RNA molecules. Nucleic Acids Res. *40*, e157.

Eberhart, D.E., Malter, H.E., Feng, Y., and Warren, S.T. (1996). The fragile X mental retardation protein is a ribonucleoprotein containing both nuclear localization and nuclear export signals. Hum. Mol. Genet. *5*, 1083–1091.

Falaleeva, M., Welden, J.R., Duncan, M.J., and Stamm, S. (2017). C/D-box snoRNAs form methylating and non-methylating ribonucleoprotein complexes: old dogs show new tricks. Bioessays *39*, https://doi.org/10.1002/bies.201600264.

Feng, Y., Absher, D., Eberhart, D.E., Brown, V., Malter, H.E., and Warren, S.T. (1997a). FMRP associates with polyribosomes as an mRNP, and the I304N mutation of severe fragile X syndrome abolishes this association. Mol. Cell *1*, 109–118.

Feng, Y., Gutekunst, C.A., Eberhart, D.E., Yi, H., Warren, S.T., and Hersch, S.M. (1997b). Fragile X mental retardation protein: nucleocytoplasmic shuttling and association with somatodendritic ribosomes. J. Neurosci. *17*, 1539–1547.

Fridell, R.A., Benson, R.E., Hua, J., Bogerd, H.P., and Cullen, B.R. (1996). A nuclear role for the Fragile X mental retardation protein. EMBO J. *15*, 5408–5414.

Henras, A.K., Plisson-Chastang, C., O'Donohue, M.F., Chakraborty, A., and Gleizes, P.E. (2015). An overview of pre-ribosomal RNA processing in eukaryotes. Wiley Interdiscip. Rev. RNA *6*, 225–242.

Incarnato, D., Anselmi, F., Morandi, E., Neri, F., Maldotti, M., Rapelli, S., Parlato, C., Basile, G., and Oliviero, S. (2017). High-throughput single-base resolution mapping of RNA 2-O-methylated residues. Nucleic Acids Res. *45*, 1433–1441.

Khandjian, E.W., Corbin, F., Woerly, S., and Rousseau, F. (1996). The fragile X mental retardation protein is associated with ribosomes. Nat. Genet. *12*, 91–93.

Kim, M., Bellini, M., and Ceman, S. (2009). Fragile X mental retardation protein FMRP binds mRNAs in the nucleus. Mol. Cell. Biol. *29*, 214–228.

Kishore, S., and Stamm, S. (2006). The snoRNA HBII-52 regulates alternative splicing of the serotonin receptor 2C. Science *311*, 230–232.

Krogh, N., Jansson, M.D., Häfner, S.J., Tehler, D., Birkedal, U., Christensen-Dalsgaard, M., Lund, A.H., and Nielsen, H. (2016). Profiling of 2′-O-Me in human rRNA reveals a subset of fractionally modified positions and provides evidence for ribosome heterogeneity. Nucleic Acids Res. *44*, 7884–7895.

Lafontaine, D.L.J. (2015). Noncoding RNAs in eukaryotic ribosome biogenesis and function. Nat. Struct. Mol. Biol. *22*, 11–19.

Li, Y., and Zhao, X. (2014). Concise review: fragile X proteins in stem cell maintenance and differentiation. Stem Cells *32*, 1724–1733.

Luo, Y., Shan, G., Guo, W., Smrt, R.D., Johnson, E.B., Li, X., Pfeiffer, R.L., Szulwach, K.E., Duan, R., Barkho, B.Z., et al. (2010). Fragile X mental retardation protein regulates proliferation and differentiation of adult neural stem/progenitor cells. PLoS Genet. *6*, e1000898.

Machnicka, M.A., Milanowska, K., Osman Oglou, O., Purta, E., Kurkowska, M., Olchowik, A., Januszewski, W., Kalinowski, S., Dunin-Horkawicz, S., Rother, K.M., et al. (2013). MODOMICS: a database of RNA modification pathways–2013 update. Nucleic Acids Res. *41*, D262–D267.

Marchand, V., Ayadi, L., El Hajj, A., Blanloeil-Oillo, F., Helm, M., and Motorin, Y. (2017). High-throughput mapping of 2′-O-Me residues in RNA using next-generation sequencing (illumina RiboMethSeq protocol). Methods Mol. Biol. *1562*, 171–187.

Muddashetty, R.S., Kelic, S., Gross, C., Xu, M., and Bassell, G.J. (2007). Dysregulated metabotropic glutamate receptor-dependent translation of AMPA receptor and postsynaptic density-95 mRNAs at synapses in a mouse model of fragile X syndrome. J. Neurosci. *27*, 5338–5348.

Muddashetty, R.S., Nalavadi, V.C., Gross, C., Yao, X., Xing, L., Laur, O., Warren, S.T., and Bassell, G.J. (2011). Reversible inhibition of PSD-95 mRNA translation by miR-125a, FMRP phosphorylation, and mGluR signaling. Mol. Cell *42*, 673–688.

Myrick, L.K., Nakamoto-Kinoshita, M., Lindor, N.M., Kirmani, S., Cheng, X., and Warren, S.T. (2014). Fragile X syndrome due to a missense mutation. Eur. J. Hum. Genet. *22*, 1185–1189.

Richter, J.D., Bassell, G.J., and Klann, E. (2015). Dysregulation and restoration of translational homeostasis in fragile X syndrome. Nat. Rev. Neurosci. *16*, 595–605.

Santoro, M.R., Bray, S.M., and Warren, S.T. (2012). Molecular mechanisms of fragile X syndrome: a twenty-year perspective. Annu. Rev. Pathol. *7*, 219–245.

Sharma, S., and Lafontaine, D.L. (2015). 'View from a Bridge': a new perspective on eukaryotic rRNA base modification. Trends Biochem. Sci. *40*, 560–575.

Shi, Z., Fujii, K., Kovary, K.M., Genuth, N.R., Rost, H.L., Teruel, M.N., and Barna, M. (2017). Heterogeneous ribosomes preferentially translate distinct subpools of mRNAs genome-wide. Mol. Cell *67*, 71–83.e7.

Shubina, M.Y., Musinova, Y.R., and Sheval, E.V. (2016). Nucleolar methyltransferase fibrillarin: evolution of structure and functions. Biochemistry (Mosc) *81*, 941–950.

Simsek, D., Tiu, G.C., Flynn, R.A., Byeon, G.W., Leppek, K., Xu, A.F., Chang, H.Y., and Barna, M. (2017). The mammalian Ribo-interactome reveals ribosome functional diversity and heterogeneity. Cell *169*, 1051–1065.e18.

Taft, R.J., Glazov, E.A., Lassmann, T., Hayashizaki, Y., Carninci, P., and Mattick, J.S. (2009). Small RNAs derived from snoRNAs. RNA *15*, 1233–1240.

Taha, M.S., Nouri, K., Milroy, L.G., Moll, J.M., Herrmann, C., Brunsveld, L., Piekorz, R.P., and Ahmadian, M.R. (2014). Subcellular fractionation and localization studies reveal a direct interaction of the fragile X mental retardation protein (FMRP) with nucleolin. PLoS One *9*, e91465.

Telias, M., Segal, M., and Ben-Yosef, D. (2013). Neural differentiation of fragile X human embryonic stem cells reveals abnormal patterns of development despite successful neurogenesis. Dev. Biol. *374*, 32–45.

ISCI, Volume *9*

Supplemental Information

FMRP Interacts with C/D Box snoRNA in the Nucleus and Regulates Ribosomal RNA Methylation

Michelle Ninochka D'Souza, Naveen Kumar Chandappa Gowda, Vishal Tiwari, Rosana Ottakandathil Babu, Praveen Anand, Sudhriti Ghosh Dastidar, Randhir Singh, Bhuvaneish Selvaraja, Rakhi Pal, Arati Ramesh, Sumantra Chattarji, Siddharthan Chandran, Akash Gulyani, Dasaradhi Palakodeti, and Ravi S. Muddashetty

Figure S1- FMRP interacts with selected set of C/D box snoRNAs in human ESCs and NPCs. (Related to Figure 1)

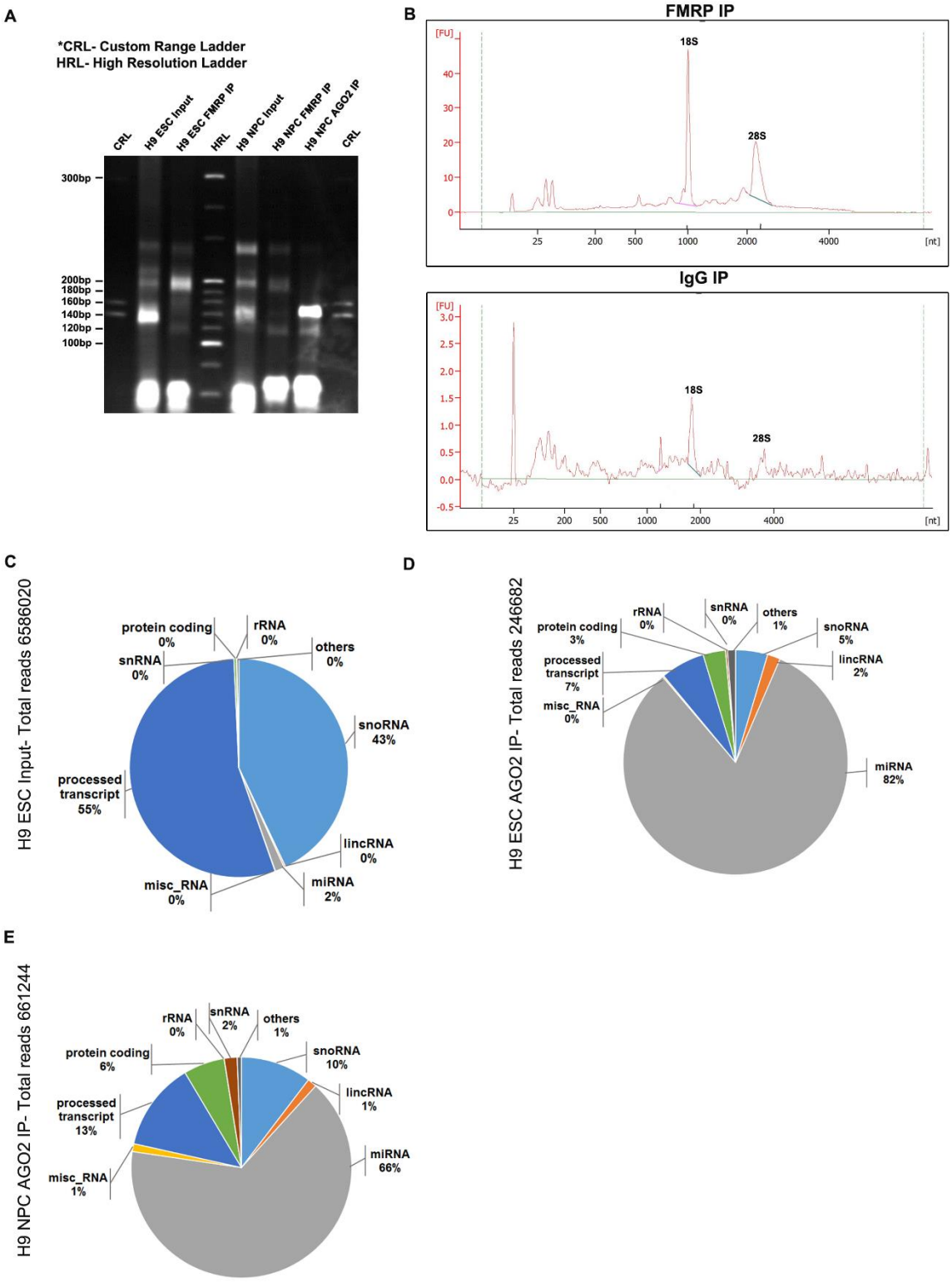

A-Polyacrylamide gels showing mobility of cDNA libraries prepared from RNA extracted after immunoprecipitation with FMRP and AGO2 from H9 hESC and hNPC lysate. **B**-Electropherogram for RNA extracted from FMRP IP (top panel) and IgG IP (bottom panel)**. C-**Pie chart representing the distribution of various kinds of RNAs in hESC input library, n=1. **D**- Pie chart representing distribution of various kind of RNAs in hESC AGO2 library, n=2. **E**- Pie chart representing distribution of various kind of RNAs in hNPC AGO2 library, n=1.

Figure S2- Validation of FMRP interaction with C/D box snoRNA. (Related to Figure 2)

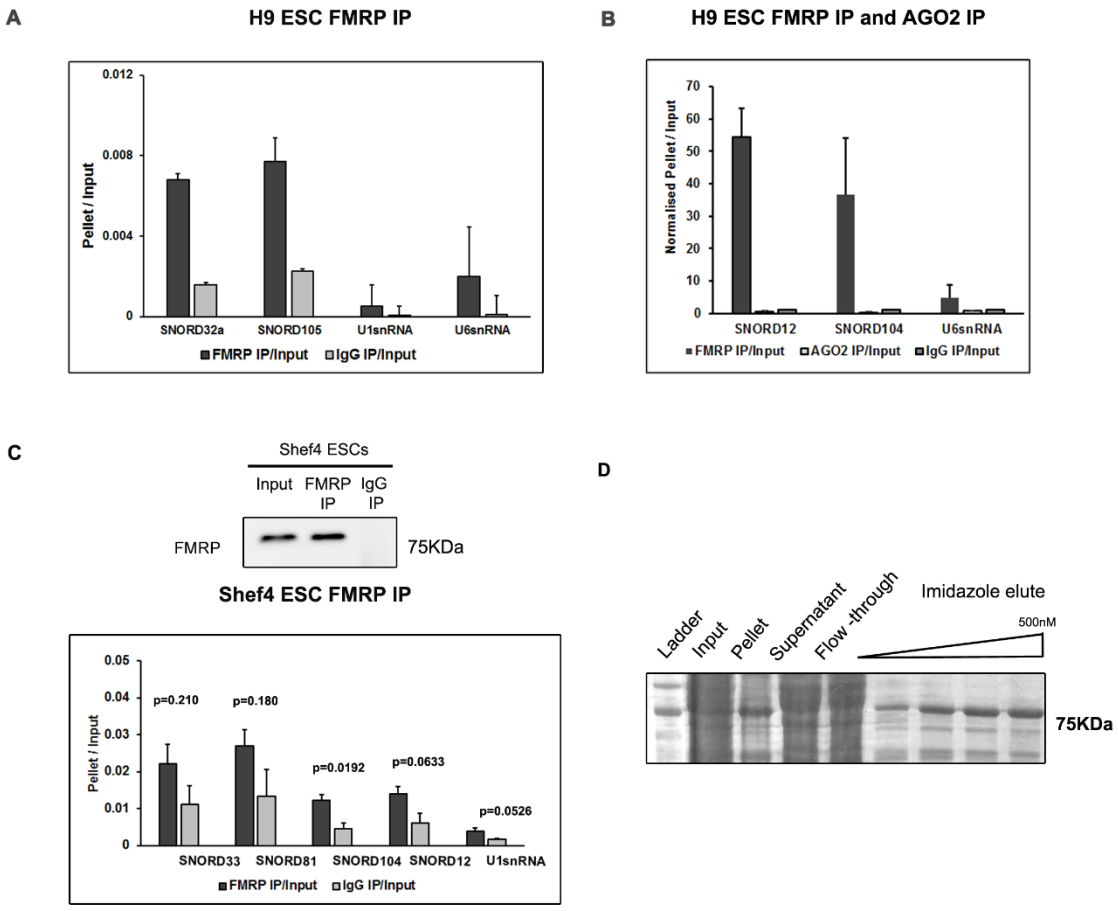

A- Validation of top snoRNA candidates in H9 hESCs with antibody raised against a different epitope of FMRP for immunoprecipitation (Sigma, F4055), n=2, mean ± SD. **B**- Validation of snoRNA candidates in H9 hESCs after FMRP and AGO2 immunoprecipitation. n=2, mean ± SD **C**- Validation of snoRNA candidates in Shef4 hESCs with FMRP immunoprecipitation (n=3, mean ± SEM, Unpaired Student's t-test). **D**- Coomassie staining of purified His-FMRP protein with varying concentrations of Imidazole containing elution buffer. Maximum elution was visualized at 500 nM Imidazole.

Figure S3- Interaction of Nuclear FMRP with C/D box snoRNA. (Related to Figure 3)

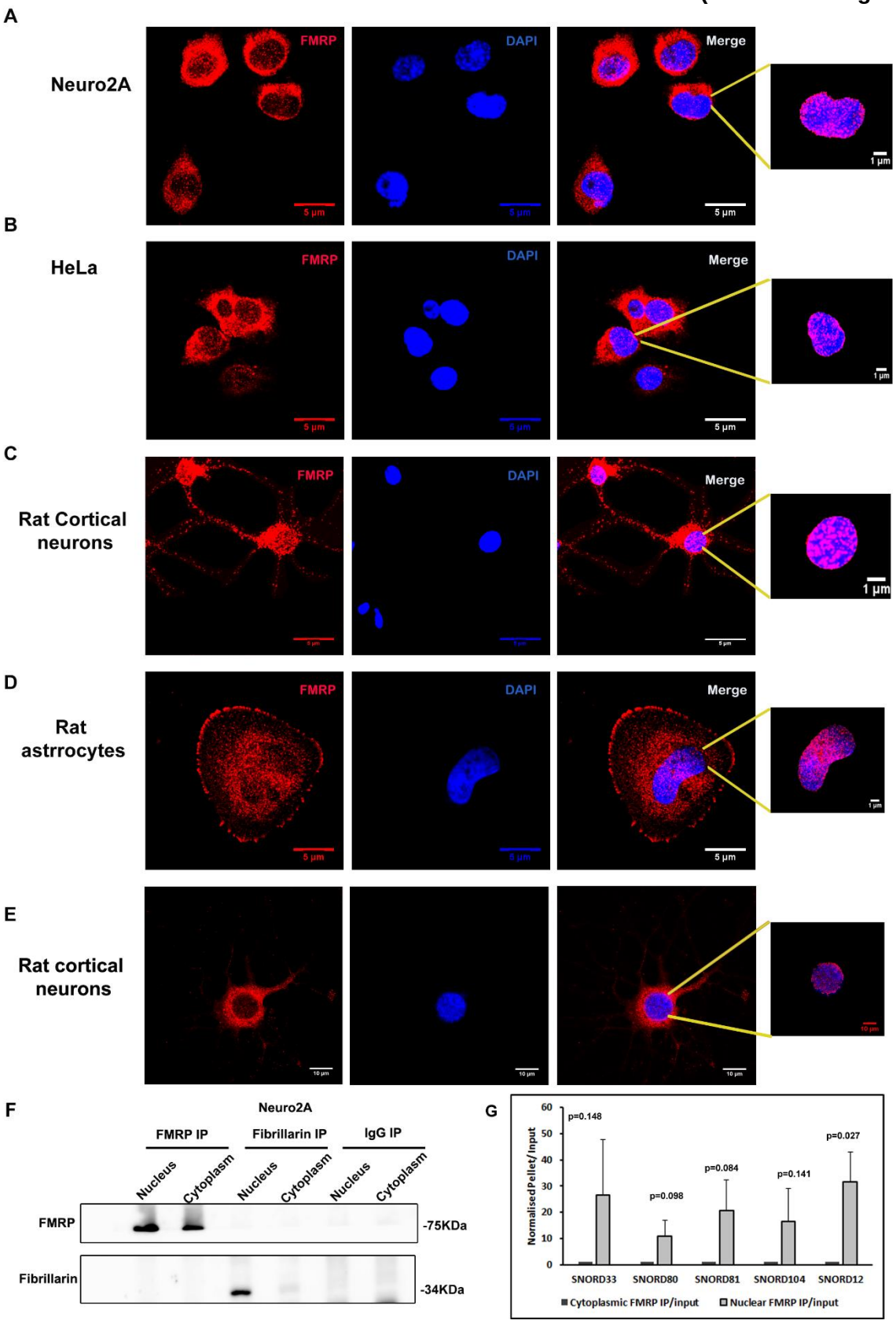

Nuclear FMRP (Red) staining in Neuro2A (**A**), HeLa (**B**), rat cortical neurons **(C**) and rat astrocytes (**D**) with DAPI (Blue) staining as a nuclear marker. Scale bar 5 µm. **E**-Nuclear FMRP (red) staining in rat cortical neurons with DAPI as a nuclear marker. Antibody used is raised against different epitope of FMRP (Scale bar 10 µm). **F**-Immunoprecipitation of FMRP and Fibrillarin in cytoplasmic and nuclear fractions of Neuro2A with IgG used as a negative control. **G-** qPCR for selected snoRNAs after immunoprecipitation with FMRP from nuclear and cytoplasmic lysates of H9 hESCs. Values are the ratio of nuclear pellet / Input normalized to the pellet/input ratio of the cytoplasmic fraction (n=3, Unpaired Student's t-test, mean ± SEM).

Figure S4- Ribosomal RNA Methylation pattern in Shef4 WT and Shef4 *FMR1* KO hESCs (Related to Figure 4)

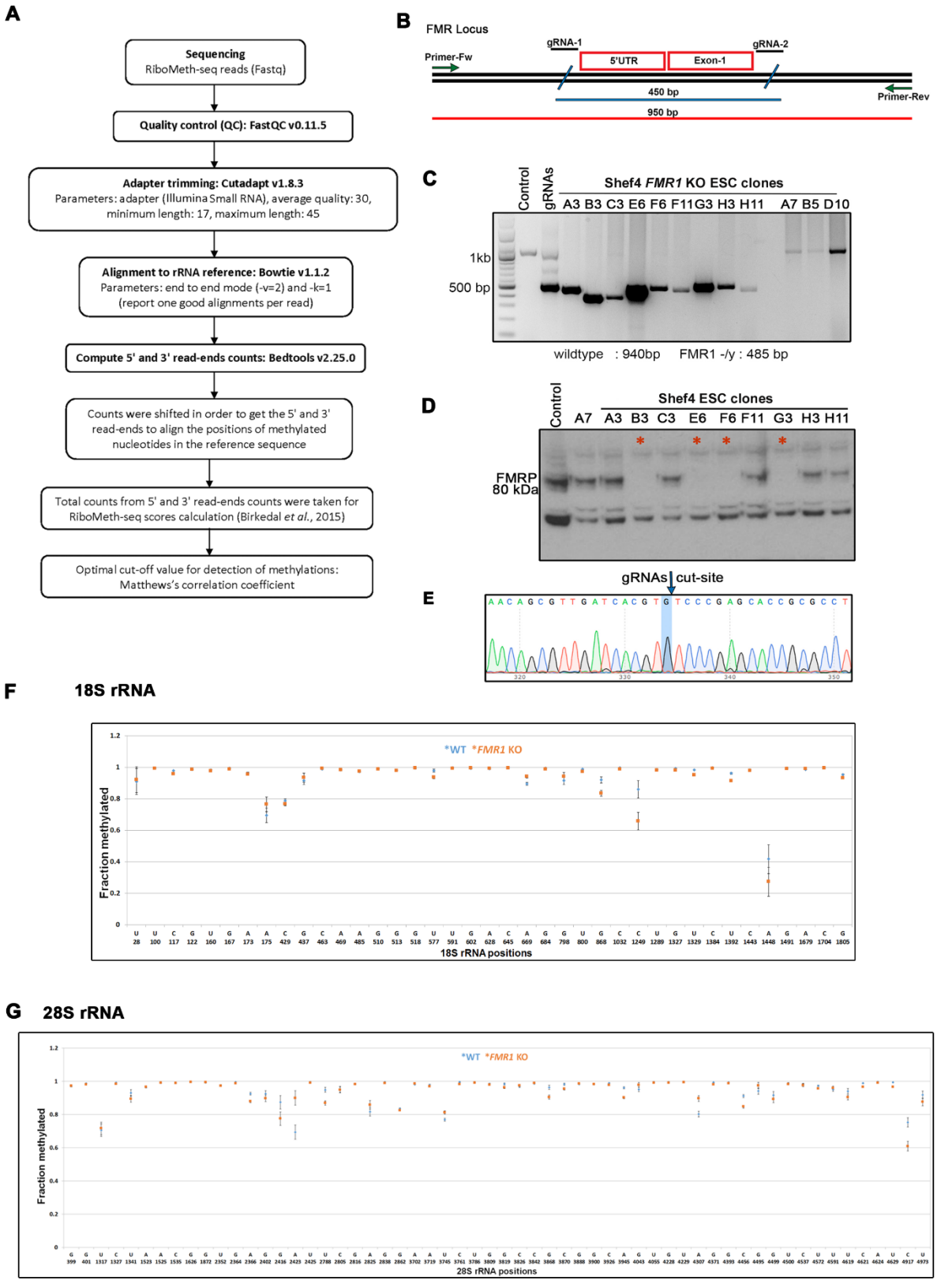

A- Pipeline for analysis of RiboMeth sequencing data indicating details of tools and parameters used for analysis. **B**-The strategy for producing *FMR1* KO hESCs with the position of the guide RNA for CRISPR/Cas9 mediated deletion. **C-** PCR screening of the clones. The positive clones have PCR amplicon of around 450 bps and the negative clones have the PCR amplicon of about 100 bp. **D-** FMRP western blot for screening the positive clones for absence of FMRP expression at protein level. The positive clones are marked by *. **E-** Representative Sanger sequence of the Shef4 *FMR1* KO hESC clone G3. **F-**Comparison of methylated fractions between Shef4 WT hESC and Shef4 *FMR1* KO hESCs along 18S rRNA. X-axis represents the respective methylation position on 18S rRNA and Y-axis represent fraction methylated, scale from 0 (min) to 1 (max), n=3. **G-** Comparison of methylated fractions between Shef4 WT hESC and Shef4 *FMR1* KO cells along 28S rRNA. X-axis represent the respective Methylation position on 28S rRNA and Y-axis represent fraction methylated, scale from 0 (min) to 1 (max), n=3.

Figure S5- Validation of change in rRNA methylation pattern by FMRP (Related to Figure 5)

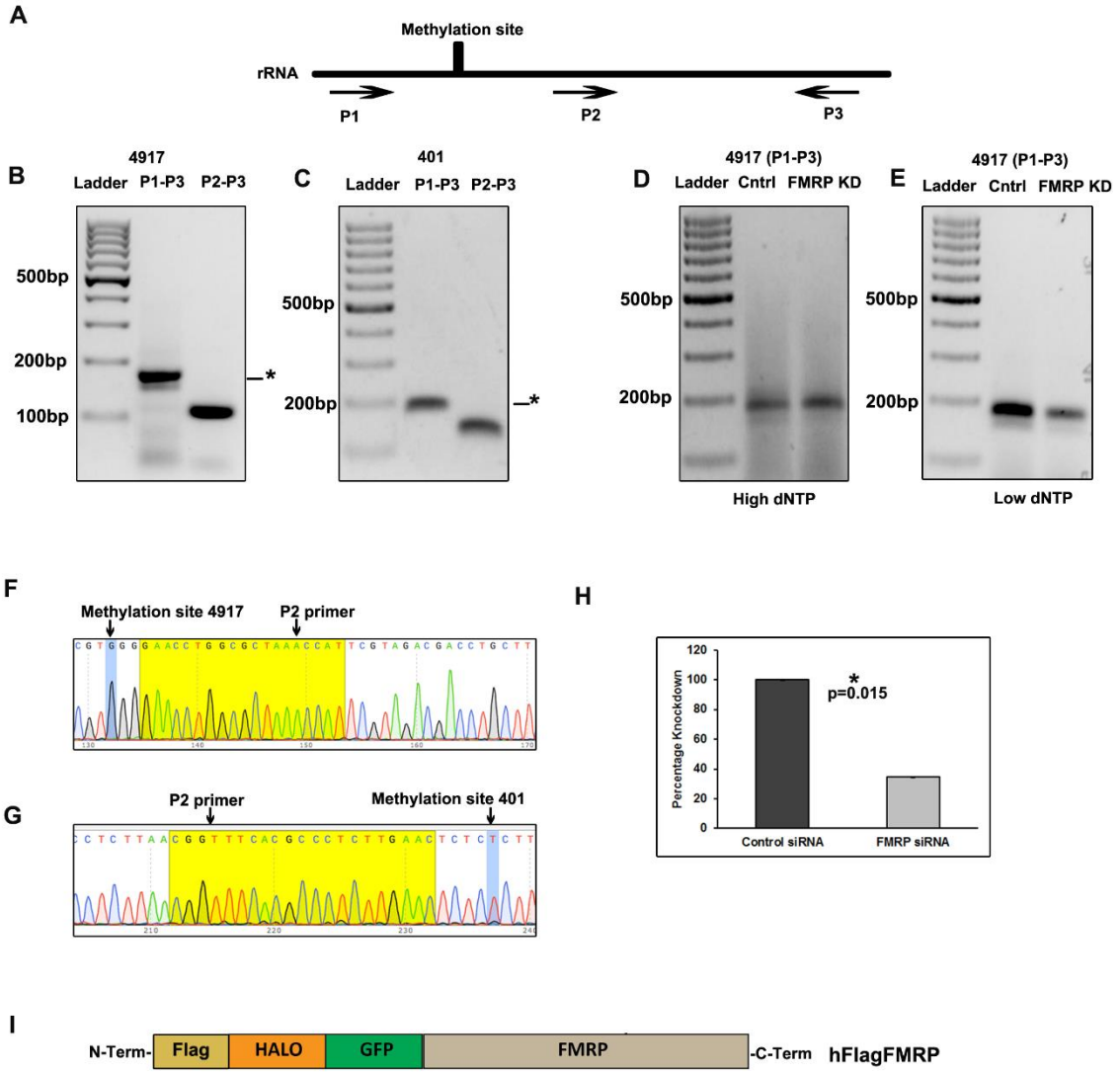

A- Schematic of primer design for RTL-P of a given position along rRNA. **B and C**-Agarose gel images representing 2'O methylation for sites 4917 and 401 along Shef4 hESC rRNA. Images show PCR products under low dNTP conditions with primers P1-P3 and P2-P3. * Indicates the band that is Sanger sequenced. **D and E**- Agarose gel images representing 2'O methylation for site 4917. PCR products were generated under low dNTP and high dNTP conditions using P1 and P3 primers. **F and G**-Ligated PCR products of methylation positions 4917 and 401 were transformed and colony selected before Sanger sequencing. Reads indicate the exact position of 2'O methylation using the downstream reverse primer (P2). **H**- Quantification of FMRP knock

down in HeLa cells (n=4, mean ± SEM, Unpaired Student's t-test). **I**- Schematic depicting the Flag-Halo-GFP-tagged WT human FMRP overexpression construct.

Figure S6- Recognition of rRNA methylation by FMRP. (Related to Figure 6)

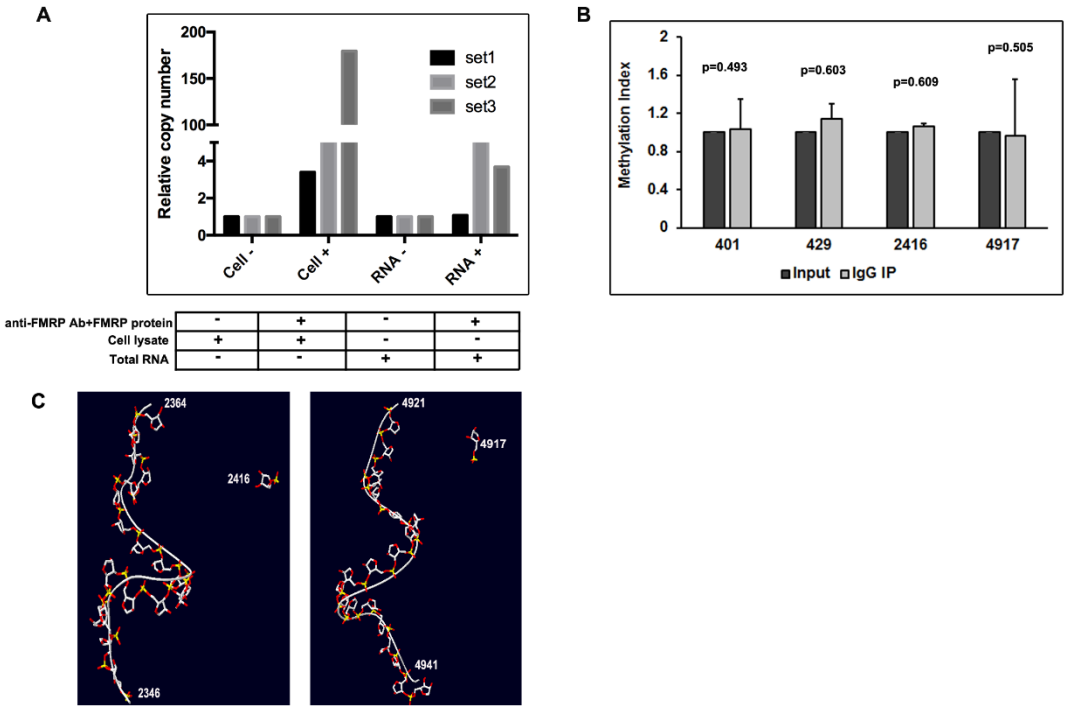

A-*In vitro* binding assay of pure human His-FMRP protein and total cell lysate / purified RNA to check the direct interaction of FMRP and 28S rRNA quantified by qPCR, Primers used were P2 and P3 corresponding to site 401. n=3. **B**- Change in methylation index between IgG IP samples and input. Plot represents values normalized to input (n=3-4, Unpaired Student's t-test, mean ± SEM). **C**- *In silico* depiction (Swiss-PDB Viewer) of 28S rRNA G-Quartet in close proximity to FMRP recognition site 2416 and 4917.

Supplementary Tables

Table S1-Enrichment of top snoRNA candidates associated with FMRP in H9 hESCs. (Related to Figure 1)

snoRNA	HGNC nomenclature		Site targeted on rRNA
U95	SNORD95	small nucleolar RNA, C/D box 95	28S rRNA A2802 and C2811
U81	SNORD81	small nucleolar RNA, C/D box 81	28S rRNA A401
U33	SNORD33	small nucleolar RNA, C/D box 33	18S rRNA U1326
U41	SNORD41	small nucleolar RNA, C/D box 41	28S rRNA U4276.
U80	SNORD80	small nucleolar RNA, C/D box 80	28S rRNA A1521 and G1612
U32A	SNORD32A	small nucleolar RNA, C/D box 32A	18S rRNA G1328 and 28S rRNA A1511
U56	SNORD56	small nucleolar RNA, C/D box 56	18S rRNA C517
U105B	SNORD105B	small nucleolar RNA, C/D box 105B	18S rRNA U799
U28	SNORD28	small nucleolar RNA, C/D box 28	18S rRNA C1391
U26	SNORD26	small nucleolar RNA, C/D box 26	28S rRNA A389
U42A	SNORD42A	small nucleolar RNA, C/D box 42A	18S rRNA U116
HBII-99	SNORD12	small nucleolar RNA, C/D box 12	28S rRNA G3878
U59B	SNORD59B	small nucleolar RNA, C/D box 59B	18S rRNA A1031
U106	SNORD12C	small nucleolar RNA, C/D box 12C	18S rRNA G1536 and U1602
HBII-202	SNORD68	small nucleolar RNA, C/D box 68	18S rRNA U428 and 28S rRNA A2388
U55	SNORD55	small nucleolar RNA, C/D box 55	28S rRNA C2791
HBII-180C	SNORD88C	small nucleolar RNA, C/D box 88C	28S rRNA C3680
U102	SNORD102	small nucleolar RNA, C/D box 102	28S rRNA G4020
U49A	SNORD49A	small nucleolar RNA, C/D box 49A	28S rRNA C4426
HBII-420	SNORD99	small nucleolar RNA, C/D box 99	28S rRNA A2774
HBII-55	SNORD110	small nucleolar RNA, C/D box 110	18S rRNA U1288
U104	SNORD104	small nucleolar RNA, C/D box 104	28S rRNA C1327
HBII-210	SNORD69	small nucleolar RNA, C/D box 69	28S rRNA G4464
HBII-99B	SNORD12B	small nucleolar RNA, C/D box 12B	28S rRNA G3878
U44	SNORD44	small nucleolar RNA, C/D box 44	18S rRNA A166
U42B	SNORD42B	small nucleolar RNA, C/D box 42B	18S rRNA U116
U25	SNORD25	small nucleolar RNA, C/D box 25	18S rRNA G1490
U57	SNORD57	small nucleolar RNA, C/D box 57	18S rRNA A99
U37	SNORD37	small nucleolar RNA, C/D box 37	28S rRNA A3697
mgh28S-2409	SNORD5	small nucleolar RNA, C/D box 5	28S rRNA C2409
SNORD119	SNORD119	small nucleolar RNA, C/D box 119	28S rRNA A4560
U18A	SNORD18A	small nucleolar RNA, C/D box 18A	28S rRNA A1313
U61	SNORD61	small nucleolar RNA, C/D box 61	18S rRNA U1442

U35A	SNORD35A	small nucleolar RNA, C/D box 35A	28S rRNA C4506
U30	SNORD30	small nucleolar RNA, C/D box 30	28S rRNA A3804
U24	SNORD24	small nucleolar RNA, C/D box 24	28S rRNA C2338 and C2352
U58B	SNORD58B	small nucleolar RNA, C/D box 58B	28S rRNA G4198
SNORD126	SNORD126	small nucleolar RNA, C/D box 126	Unknown target
U75	SNORD75	small nucleolar RNA, C/D box 75	28S rRNA C4032
U43	SNORD43	small nucleolar RNA, C/D box 43	18S rRNA C1703

Table S2-Top snoRNA candidates showing more than 2 fold enrichment in the FMRP pulldown when compared to the input. (Related to Figure 1)

Top snoRNA	FMRP IP	Input
U95	102760	2437
U81	154548	4531
U33	53353	2386
U41	25018	1313
U80	106248	5953
U32A	48269	3992
U56	10909	1053
U105B	179656	18161
U28	11161	1321
U26	45306	5622
U42A	326677	43105
HBII-99	412639	64471

Values indicate the un-normalized raw reads of respective snoRNA in the Input (n=1) and the mean un-normalized raw reads for the FMRP IP (n=3).

Table S3-Sites showing at least 5% change in methylation on rRNA.(Related to Figure 4)

rRNA	Methylated position	Methylation index	
		WT	KO
18S	A175	0.695	0.765
	C429	0.789	0.767
	A669	0.895	0.941
	G868	0.919	0.833
	C1249	0.860	0.657
	T1392	0.961	0.914
	A1448	0.417	0.274
28S	A2366	0.924	0.879
	G2416	0.874	0.775
	T2788	0.949	0.869
	A2825	0.817	0.858
	T3745	0.769	0.812
	G3868	0.963	0.904
	A3945	0.962	0.902
	A4307	0.803	0.897
	C4456	0.911	0.847
	C4917	0.753	0.609

Transparent Methods

Ethics Statement

All the work was done with due approval from the Institutional Animal Ethics committee (IAEC) and the institutional biosafety committee (IBSC), InStem, Bangalore, India.

Generation of Shef4 *FMR1* KO cells

Shef4 *FMR1 KO* hESCs were generated using CRISPR-Cas9 technology (**Figure S4C-G**). The gRNA sequences used to delete 450 bp region which includes the 5'UTR and exon 1 for generating the knockout are as follows-

FMR1 gRNA Fw: 5'-cagcgttgatcacgtgacg-3'

FMR1 gRNA Rev: 5'-ggcgcggtgctcgggaaga-3

Clones were screened through PCR where the positive clones have PCR amplicon of around 450bps and the negative clones have the PCR amplicon of about 100bp. Western blots for the screened positive clones showed absence of FMRP expression at protein level. The positive clones are marked by *. *FMR1* KO hESC clone G3 which was used for experiments was Sanger sequenced further

Cell line and Embryonic Stem Cell culture

H9 hESCs were cultured on Matrigel (BD Biosciences, 3545277) coated plates containing mTeSR1 medium (StemCell Technologies, 5850) at 37°C in a 5% CO2 environment. Cells were further passaged with an enzyme cocktail containing 1 mg/ml of Collagenase type IV (Invitrogen), 20% KOSR (Gibco), 0.25% Trypsin and 1 mM $CaCl_2$ dissolved in 1X PBS without $CaCl_2$ or $MgCl_2$ pH 7.2. For immunostaining experiments, H9 hESC colonies were plated on Matrigel coated glass coverslips and cultured as mentioned above.

H9 hESCs were further differentiated to Neural Precursor Cells (hNPCs) by inducing them with medium containing DMEM/ F12/ Advanced neurobasal medium (1:1), 1% N2, 1% B27 without Retinoic acid, 1% L-glut,0.1% Pen/Strep and the inhibitors SB431542 (SMAD inhibitor 10µM) and LDN193189 (Noggin analog 0.1 µM) for 14 days. The hNPCs were further expanded in medium containing DMEM/F12 / Advanced neurobasal medium(1:1), 1% N2, 1% B27 without retinoic acid, 1% L-glut,0.1% Pen/Strep , FGF2 (10 ng/ml) and EGF (10 ng/ml) (Shi et al., 2012).

Shef4 WT and Shef4 *FMR1* KO hESCs were maintained on Matrigel coated plates containing Essential 8™ Medium (ThermoFisher Scientific (A15169-01) and passaged with a 1:1 solution of 2 mg/ml Collagenase type IV (Gibco 17104-019) and 1 mg/ml Dispase (Gibco 17105-041). Collagenase and Dispase stock solutions were prepared in Advanced DMEM-F12 (Gibco 12634-010).

HeLa and Neuro2A cells were maintained in DMEM containing 10% FBS and 1% Penicillin-Streptomycin at 37°C in a 5% CO2 environment passaged using 0.05% trypsin-EDTA solution. Primary neuronal cultures were prepared from E18 rat pups (Sprague Dawley) according to an established lab protocol (Kaech and Banker, 2006). Neurons were dissociated and cultured on Poly-l-lysine coated coverslips in defined Neurobasal Medium supplemented with B-27 and Glutamax. Neurons were cultured for 5 days at 37°C in a 5% CO2 incubator (low density 2500 cells per sq.cm). Astroglia were obtained from the same animal as that of the neurons and grown in MEM supplemented with 10% FBS and 1X Glutamax for 2 weeks.

Immunostaining

Cells were fixed with 4% PFA before staining. The cells were permeabilized with TBS-50T (0.3 %) [50 mM Tris-Cl (pH 7.4), 150 mM NaCl, 0.3% TritonX-100] followed by treatment with Tris-Glycine solution (0.5 M Tris and 0.2 M Glycine). The cells were blocked with buffer containing 2 % BSA and 4 % FBS. Cells were incubated with primary antibody overnight at 4°C and Alexa fluor coupled anti-mouse 488 and anti-rabbit 555 secondary antibodies at room temperature for 2 hours. The cells were finally incubated with DAPI for 5mins before being mounted with Mowiol® 4-88 mounting medium. For quantification of FMRP in hESCs, Images were acquired on Olympus FLUOVIEW 3000 confocal laser scanning microscope (Olympus Corporation) with 60X PlanApo N, NA- 1.42, oil immersion objective. For maximum resolution both in the XY direction and Z direction, Images were acquired using optical zooming of 2.5x to satisfy the sampling theorem of Nyquist, pinhole was kept at 1 Airy unit and stacks in the Z direction were acquired with a step size of 0.3µm. Imaging conditions were kept constant across different data sets, across experiments.

Image Analysis: Image analysis was done Bitplane IMARIS 9.0 (Bitplane, oxford Instrument Company) software. For quantifying intensity within the nucleus, DAPI Channel was used to make volumetric nuclear mask and FMRP channel was used to make volumetric mask the entire cell. Local background correction was done using a radius of 5-10 µm while making the masks. Subsequently, integrated intensity was calculated for FMRP channel within both nuclear mask and whole cell mask and was plotted as a ratio of nuclear and cytoplasmic intensity for multiple cells from 3 independent experiments. The distribution was then checked for normality.

Immunoprecipitation

Cells were lysed in a 1 % NP40 containing lysis buffer (20 mM Tris-HCl pH 7.5, 150 mM NaCl, 5 mM $MgCl_2$ with protease and RNase inhibitors) and spun at 18000 rcf (12500 rpm) for 20 minutes

at 4°C. Precleared supernatant was used for immunoprecipitation with Protein G Dynabeads. 5 µg of anti-FMRP/ AGO2/ Fibrillarin/Flag antibody was coupled to the Protein G Dynabeads. Similar amount of normal mouse/rabbit IgG antibody was used as a control.

Cellular fractionation

H9 hESCs and HeLa cells were trypsinised (0.25 % trypsin) and centrifuged down at 1000 rpm for 5 minutes at 25°C. The pellet was lysed with a 0.1% NP40 containing lysis buffer (20 mM Tris-Cl pH 7.4, 150 mM NaCl, 10 mM $MgCl_2$, 1 mM DTT) with gentle trituration. 1/3rd of the volume was spun down at 10,000 rpm and the supernatant was used as the cytoplasmic input. The remaining 2/3rd of the lysate was gently layered over a 1 M sucrose cushion and spun at 2800 g for 20 minutes at 4°C. The final nuclear pellet was suspended in a 1 % NP40 containing lysis buffer and used for further experiments.

Small-RNA sequencing

H9 hESCs and hNPCs were lysed with a 1 % NP40 containing buffer and centrifuged at 18000 rpm for 20 minutes at 4°C. The supernatant obtained was used for immunoprecipitation with FMRP and AGO2 antibodies at room temperature for 1hour. Whole cell lysates were used to generate input libraries which were also sequenced. Antibody bound RNA was extracted from the respective pellets using the Trizol method of extraction. Isolated RNA was used for library preparation using TruSeq small RNA library kit from Illumina (Cat- RS-930-1013). The prepared libraries were resolved on a 6 % PAGE gel with TBE buffer. Bands corresponding to 150 bp and 200 bp were excised out and separately sequenced by HiSeq 1000.

Analysis of small-RNA sequencing

The raw reads from each of this library were uniformly processed. The first step involved removal of adapter sequence (5’ TGGAATTCTCGGGTGCCAAGG 3’) from the reads using cutadapt (Martin, 2011) with the parameters –q 30 (quality score) and –minum-length 36 (minimum length of the read after trimming). The trimmed and processed reads were then further analyzed to filter out the reads corresponding to rRNA. The gencodeV19 was used to derive the sequences of rRNA from hg19 version of the genome and the reads that mapped to these rRNA sequences were removed. The remaining reads were then aligned to the genome using the bowtie (Langmead et al., 2009) with parameters ‘-q --best -m 1 -k 1 --chunkmbs 200’ to ensure that unique reads are mapped to the genome. The total number of reads in the library, trimmed, filtered and aligned are tabulated in **Supplementary Table 2**. The ‘Homo_sapiens.GRCh37.75.gtf’

annotation was used to derive the counts for individual features using HTSeq (Anders et al., 2015). The MDS plot for these 10 samples were derived using edgeR package in R (Robinson et al., 2010). The PCA plot measures the similarity of the samples and projects this measure on to two dimensions. A filter of at least 1 read per million in at least one of the ten samples was used for PCA analysis. In all the FMRP pull down libraries, on average 33% of the reads were associated with snoRNAs. The aligned bam files generated were converted to bed and the overlap analysis with the annotated snoRNAs in UCSC genome browser was performed using bedtools (Quinlan and Hall, 2010) to get the counts for each type of snoRNA.

RiboMethSeq and analysis

Total RNA from Shef4 WT and Shef4 *FMR1* KO cells was extracted and 2 µg of RNA was used for library preparation. Further, RNA was hydrolysed with an alkaline Tris buffer, pH 10 at 95°C for 5 minutes. Hydrolysed RNA was precipitated by ethanol and run on a 12 % PAGE gel with TBE as running buffer. After separation, the band around 30-50 bp was excised out **(Figure 1D and Figure S1A)**. The library was prepared according to the TruSeq small RNA library preparation protocol from Illumina and sequencing was done on Hiseq 3000 instrument. Preliminary trimming of adapter sequence was done using Cutadapt v1.8.3 (Martin, 2011) with the following parameters: adapter (Illumina Small RNA), average quality: 30, minimum length: 17 bp, maximum length: 45 bp. Alignment to the reference rRNA sequence was done by Bowtie v1.1.2 (Langmead et al., 2009) with parameters: -v=2 (end-to-end mode) and k-1 (one good alignment per read). Computed the number of 5' read-ends and 3' read-ends that are mapped to each positions of reference rRNA using Bedtools v2.25.0. The 5' and 3' read-ends counts were shifted to obtain the actual methylated positions based on the alignment to methylated nucleotide in the reference sequence. Ultimately, two datasets from 5' and 3' read-ends counts were combined for calculation of RiboMeth-seq scores. Optimal cut-off values for detection of methylations were determined using Matthews's correlation coefficient using ROCR package (Sing et al., 2005).

Data Availability

Sequencing data for both Shef4 hESC RiboMethseq and H9 hESC snoRNA have been deposited at NCBI Genbank under the following identifiers.

RiboMethseq- https://www.ncbi.nlm.nih.gov/bioproject/?term=PRJNA407420

snoRNA- https://www.ncbi.nlm.nih.gov/bioproject/?term=PRJNA407706

Constructs

Human FMRP gene was amplified (1900bp) from Addgene plasmid (cat no #48690) and sub cloned into EGFP-C1 vector named as EGFP-FMRP. The gene encoding HALO tag was inserted before EGFP sequence of EGFP-FMRP construct using Overlap extension PCR to give Flag-HALO-EGFP-FMRP (Flag-FMRP) which was used for over expression experiments. Full length human FMRP gene was again cloned into pET28a+ bacterial expression vector along with a 6X His tag which was used for protein expression and purification later.

Overexpression or knockdown experiments

Flag-FMRP construct was transfected to HeLa cells using Lipofectamine 2000transfection reagents as per manufacturer instruction (Invitrogen, 11668019) and incubated for 24 hours. The over-expression of these constructs was confirmed by the presence of GFP fluorescence using fluorescence microscope (IX 73, Olympus).Knockdown of FMRP was performed using *FMR1*-siRNA with Lipofectamine 2000 transfection reagent and incubated for 48 hours. Knockdown was confirmed by western blotting and comparing against α-Tubulin.

FMRP expression and purification

Human FMRP with 6X His tag was cloned in a pET28a vector and transformed into Rosetta DE3 competent cells. Cells were incubated overnight in the presence of kanamycin (50ug/ml). The expression of FMRP ISO1 was induced in 4lt of culture with isopropyl β-D-1-thiogalactopyranoside (IPTG) at a final concentration of 0.5 mM for 16 hours at 18^{o}C. The final bacterial pellet was lysed in buffer containing 20 mM HEPES pH 8.0, 500 mM NaCl, 10 mM $MgCl_2$, 10 mM β-mercaptoethanol, 10% glycerol. Clarified bacterial lysate was added on to an equilibrated Ni-NTA column (Life Technologies, R90115). Purified His-FMRP was eluted in fractions using buffer containing a gradient of 100 mM to 500 mM imidazole. Protein stocks were dialysed to remove the imidazole, concentrated and flash frozen with 10% glycerol.

RNA labelling and EMSA

SNORD80 was in vitro transcribed using recombinant T7 RNA polymerase purified in the lab. This was treated with Calf Intestinal alkaline Phosphatase (NEB M0290S) and 5'end labelled with γ-[^{32}P] ATP. Nonspecific bacterial RNA was *in vitro* transcribed in a similar manner. Radiolabeled RNA (~10 fmol @ 20 CPS/µl) was incubated with increasing amounts of His-FMRP in buffer containing 25 mM Tris Ph8, 5 mM $MgCl_2$, 10% glycerol 2 mM DTT and 150 mM NaCl in the

presence of 2.5 ng/µl yeast tRNA and 10 U of RNAseOUT for 1 hour at RT. 10 M (280 pmoles) excess of unlabeled SNORD80 was used in a reaction to compete out the binding between radiolabeled SNORD80 and the maximum concentration of His-FMRP (14.6 µM). 7 µl of the reaction mixture were loaded in IX TBE / 5% native gel (5% acrylamide: bis (80:1). and run at 100V for approximately 40 minutes in cold. The gel was dried and exposed overnight using Typhoon FLA 7000 Phosphorimager.

Validation of RTL-P assay.

PCR amplification of the RTLP products was performed using methylation specific forward and reverse primers. 2 µL of reaction products was run on 3% agarose gel and imaged using Amersham Imager 600. Specific bands were cut out from the gel and purified (QIAquick, 28704). Product was re-ligated into a vector (pCR2.1 -TOPO) using the TOPO TA cloning standard protocol. Positive (white) colonies were selected and propagated. Plasmids were isolated (Qiagen plasmid Miniprep isolation spin, 27104) and subjected to Sanger sequencing.

***In vitro* RNA immunoprecipitation**

Shef4 *FMR1* KO ESCs cells were lysed in a 1 % Triton-X 100 containing 1X EMSA buffer and spun at 18000 rcf for 20 minutes at 4°C to clear the lysate. Similarly hESC total RNA was extracted using Trizol LS. 5 µg of anti-FMRP antibody was coupled to Protein G Dynabeads at RT for 30 min followed by equimolar concentrations of purified FMRP protein which was incubated for 30 min at RT. For immunoprecipitation, equimolar concentration cell supernatant or RNA was incubated with the protein bound beads for 30 min at RTwith 1X EMSA buffer. RNA was eluted and rRNA quantified by qPCR.

RTL-P (*Reverse transcription at low-dNTP concentration followed by PCR*)

2 ng of sample RNA was used for cDNA preparation using reverse primers (10 µM) specific to methylation sites under high dNTP (10 mM) and low dNTP (1 nM) concentrations. For real time PCR, we adopted a method from (Dong et al., 2012). We have used two forward primers for a methylation site; one up-stream (P1) and one down-stream (P2) from the methylation site, along with a common reverse primer (P3). Amplification with these sets of primers would yield one product over the methylation site which will be the longer product and other will be within the methylation site and would yield a small length product (**Figure S5A**). The extent of methylation at a given site was measured as an RTLP as mentioned below.

RTLP score calculation

Ct low- Ct High (Upstream primer) =X

Ct low- Ct High (Downstream primer) =Y

Ribometh score = 2^ (X-Y)

The RiboMeth score is then normalized to corresponding control (WT vs KO, Input vs IP).

Example of calculation of methylation index for a site 4917 on 28S by RTL-P

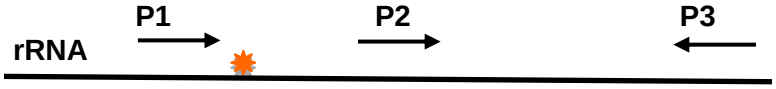

Step 1: Ct values for each site with methylation specific upstream and downstream primer are done using high and low dNTP concentration.

	P1-P3	P1-P3	P2-P3	P2-P3
High dNTP	19.21	19.35	13.88	13.57
Low dNTP	23.59	23.23	15.34	15.38
NTC	34.23	32.08	31.97	36.94

Step 2: Average of the Upstream and downstream Ct values

	P1-P3 (x)	P2-P3 (y)
High dNTP	19.28	13.72
Low dNTP	23.41	15.36
NTC	32.08	31.97

Step 3: Subtract the Upstream Ct value from the Downstream Ct value

	y-x
High dNTP	5.5576
Low dNTP	8.05

Step 4: Subtract the High dNTP values from Low dNTP value

	Low-High
WT	2.4934

Step 5: **2^-(Low-High)** the value from step 4

	2^- (Low-High)
Un-normalized Methylation Index	5.631

Table above represents the value of absolute methylation index. Further, we can calculate relative methylation index based on considered normalization factor.
WH -Wild type High
WL -Wild type Low
NTC – No template control

Statistical Analysis

Statistical significance was calculated using Unpaired Student's t-test for all biochemical and qPCR assays. For imaging quantifications, distribution of data points was assessed using Shapiro-Wilk's test. For RiboMethseq, Matthew's correlation coefficient was used to obtain values with an optimal cut-off to detect the 2'O- Methylation. All data was plotted as Mean ± SEM unless mentioned otherwise. Values with $p<0.05$ was considered statistically significant.